Reviews in Physics 5 (2020) 100043

Contents lists available at ScienceDirect

Reviews in Physics

journal homepage: www.elsevier.com/locate/revip

The advancement of blood cell research by optical tweezers

Tatiana Avsievich[a], Ruixue Zhu[a], Alexey Popov[b], Alexander Bykov[a], Igor Meglinski*[,a,c,d,e,f]

[a] Optoelectronics and Measurement Techniques, University of Oulu, 90570, Finland
[b] VTT Technical Research Centre of Finland, Oulu 90590, Finland
[c] Interdisciplinary Laboratory of Biophotonics, National Research Tomsk State University, Tomsk 634050, Russia
[d] Institute of Engineering Physics for Biomedicine (PhysBio), National Research Nuclear University (MEPhI), Moscow 115409, Russia
[e] School of Engineering and Applied Science, Aston University, Birmingham B4 7ET, UK
[f] School of Life and Health Sciences, Aston University, Birmingham B4 7ET, UK

ARTICLE INFO

MSC:
41A05
41A10
65D05
65D17
Optical tweezers
Red blood cells (RBCs)
RBC biomechanics
RBC interactions
leukocytes (white blood cells)
Platelets

ABSTRACT

Demonstration of the light radiation pressure on a microscopic level by A. Ashkin led to the invention of optical tweezers (OT). Applied in the studies of living systems, OT have become a preferable instrument for the noninvasive study of microobjects, allowing manipulation and measurement of the mechanical properties of molecules, organelles, and cells. In the present paper, we overview OT applications in hemorheological research, placing emphasis on red blood cells but also discussing OT applications for the investigation of the biomechanics of leukocytes and platelets. Blood properties have always served as a primary parameter in medical diagnostics due to the interconnection with the physiological state of an organism. Despite blood testing being a well-established procedure of conventional medicine, there are still many complex processes that must be unraveled to improve our understanding and contribute to future medicine. OT are advancing single-cell research, promising new insights into individual cell characteristics compared to the traditional approaches. We review the fundamental and practical findings revealed in blood research through the optical manipulation, stretching, guiding, immobilization, and inter-/intracellular force measurements of single blood cells.

1. Introduction

The elegant physical experiment by Arthur Ashkin [1] at Bell Labs demonstrated that light radiation can exert pressure on material microobjects that is strong enough to move them. Prior to this, J. Kepler assumed that solar pressure acted on the tail of a comet, forcing it to point away from the sun [2]. The theoretical background for this idea was provided by Lebedev [3]. However, years later, the invention of the laser made it possible to experimentally confirm this idea.

In 1970, Askin observed the attraction of small dielectric particles to the midpoint of an unfocused Gaussian laser beam together with their acceleration in the direction of beam propagation, known today as optical guiding. Based on this discovery, he further demonstrated the stable particle trapping at the midpoint of a set of two counterpropagating beams, trapped by the pressure from both of them, which was a prototype of the modern dual-beam trap. Eventually, in 1986, Arthur Ashkin, together with Joseph Dziedzic, John Bjorkholm, and Steven Chu, performed the first particle trapping - holding and moving a particle in three dimensions with a highly focused laser beam. This method, named the “single-beam gradient force trap” [4], was considered a major

* Corresponding author.
E-mail address: i.meglinski@aston.ac.uk (I. Meglinski).

https://doi.org/10.1016/j.revip.2020.100043
Received 4 October 2019; Received in revised form 21 May 2020; Accepted 22 May 2020
Available online 06 June 2020

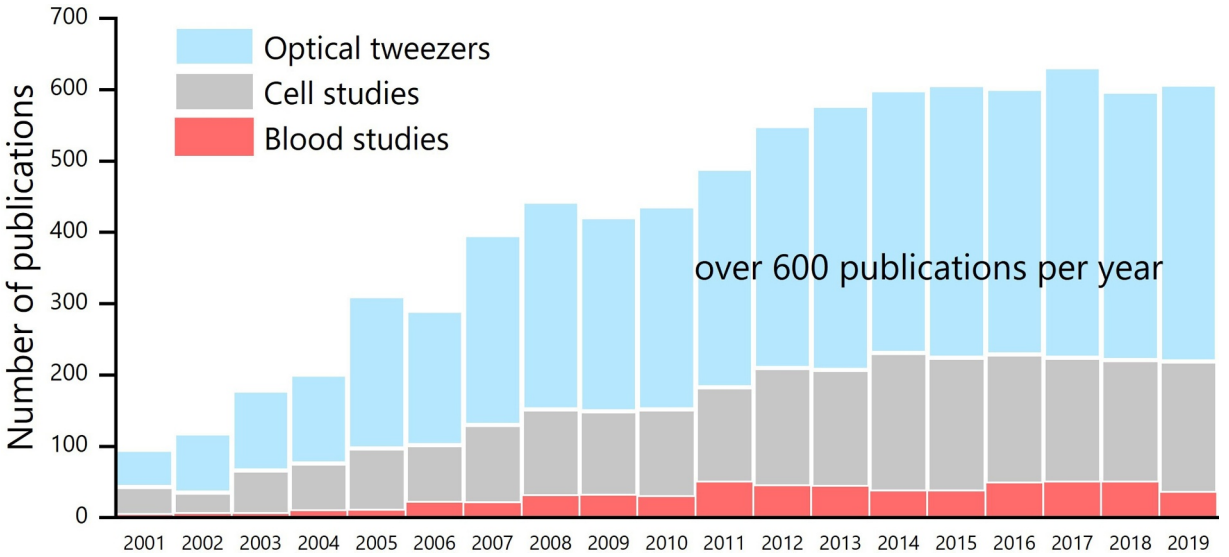

Fig. 1. Number of publications on OT in general and applications of OT in cell and blood studies, according to a data search on the Web of Science database.

breakthrough and marked the beginning of the optical micromanipulation field. Currently, this technique is commonly called optical tweezers (OT).

OT have made a drastic contribution to the natural sciences, offering abundant opportunities to study nano- and micro-sized objects in physics and biology. OT enable the noninvasive manipulation of biomolecules (protein and DNA), viruses, bacteria, and cells and have been proven to be safe for living objects [5]. As expected, in 2018, Arthur Ashkin was recognized by the Nobel Prize for the creation of OT and their application to biological systems [6]. According to the Web of Science database, within the last 6 years, the number of publications on OT has grown to 600 per year (Fig. 1). Almost half of these publications are devoted to cell studies.

Cellular activities, function and functional disorders are crucially dependent on the mechanical properties of cell structures; hence, the use of OT became a classical approach for single-cell investigations [7,8]. The advantages of OT compared to micropipette aspiration and atomic force microscopy (AFM) are higher sensitivity, control over a whole cell in a nondestructive manner, no risk of contamination, and simple control of the laser light intensity to adjust the applied force with an accuracy down to piconewtons.

In the present review, we attempt to summarize the main studies involving OT in hemorheology. Human blood is a life-sustaining fluid that provides all organic systems with oxygen and nutrients and removes by-products. Moreover, blood components are responsible for the immune response of an organism. The mechanical properties of whole blood or its components have the potential to be utilized as label-free biomarkers of the physiological state of an organism. Routine analysis of blood relies on established methodologies. Conventional methods for blood analysis currently include complete blood count (CBC), blood glucose and cholesterol tests, which provide averaged data over a bulk cell suspension. Individual cell analysis methods, however, are always more sensitive to small differences than those based on bulk samples of cells. Thus, optical trapping can reveal the intercellular heterogeneity and complement blood tests. OT in blood research allow the single-cell-level study of cell-cell interactions, aggregation, infectious disorders, and immune-related processes.

Red blood cell (RBC) biomechanical properties arise from their unique deformability, which enables them to travel through the smallest capillaries of the human body. Being relatively simple structures of the phospholipid bilayer membrane and lacking nuclei and some organelles, RBCs have often been used as a model system for cell mechanodynamics studies, revealing the interrelation between structural, chemical, and biological signals and the corresponding mechanical response [9]. OT approaches are directed toward studying, at first, intrinsic RBC properties, particularly deformability and viscosity, and cell-to-cell interactions, for example, aggregation and adhesion. Experimental implementations involve mainly the trapping of a whole cell, such as in sorting [10–15], optical stretchers [16] and rotators [17], or exerting a force through microbeads attached to the membrane [18]. The OT method is a great instrument on its own, but combinations with other modalities, such as Raman spectroscopy [19,20], fluorescent microscopy [21], microfluidics [22–24], etc., have largely enhanced its potential in fundamental and practical applications.

The mechanical features of leukocytes and platelets are crucial for the immune response of an organism and interdependent with a variety of chemical mediators. The application of OT for leukocyte and platelet studies is limited due to the high sensitivity of cells to mechanical forces, resulting in cell activation. Therefore, OT are not used for passive behavior studies of leukocytes and platelets. Nonetheless, the technique was found to be a powerful tool in studies of immune cells as neutrophils [25] and T-lymphocytes [26].

Given the number of accumulated research results, OT is currently expected to be applied to medical diagnostics. Therefore, the technique is evolving to fill the requirements of high sensitivity, portability, uniform standards, and fast measurement procedures for many practical applications, which are still challenging, especially for in vivo experiments.

Here, we review the contributions OT have made to hemorheological research, starting from the first implementation for RBC

trapping, the recent applications to leukocytes and platelets, and finally in vivo optical manipulation. OT technical implementations are presented throughout the review regarding the findings they yielded when applied to blood cells.

2. Fundamental principles of optical trapping

The fundamental physical principles of optical trapping, along with its design, have been thoroughly covered in a number of comprehensive reviews [27–32], and the diversity of OT applications has been reviewed [33–35].

In the simplest scenario, a small dielectric spherical particle of radius r in the field of a focused laser beam with a wavelength λ is considered. The forces acting on the particle from the laser beam arise from the momentum P carried by the photons and exchanged with the trapped particle, the refractive index of which is higher than that of the surrounding medium, $n_p > n_m$ [36]. This results in the reaction net force:

$$F = Qn_m/c, \tag{1}$$

where Q is the trapping efficiency, n_m is the refractive index of the medium surrounding the object, and c is the velocity of light.

The optical forces exerted on the particle originate from the combined action of two forces - gradient and scattering. The gradient force is induced by the gradient of the Gaussian laser beam intensity and is directed toward the beam focus, while the scattering force is caused by the photons hitting the object in the beam direction, driven by the reflection and refraction of light. The trapping force depends on the size and the shape of the particles, the refraction index n_p of the particle relative to the n_m of the environment (medium), and the trapping laser characteristics, such as the intensity, beam shape, and focal point. The ratio between the particle size, expressed through the radius r, and the wavelength of the trapping laser defines the relevant physical phenomenon behind the trapping process.

1) The simplest approach corresponds to the case where the particle size is substantially larger than the wavelength of the laser source, $r > > \lambda$. This process can be described in the frame of geometrical optics or the Mie regime [27], as shown in Fig. 2(a). A particle, being transparent for light beams, will behave as a lens focusing the incident light. By tracing individual rays from the

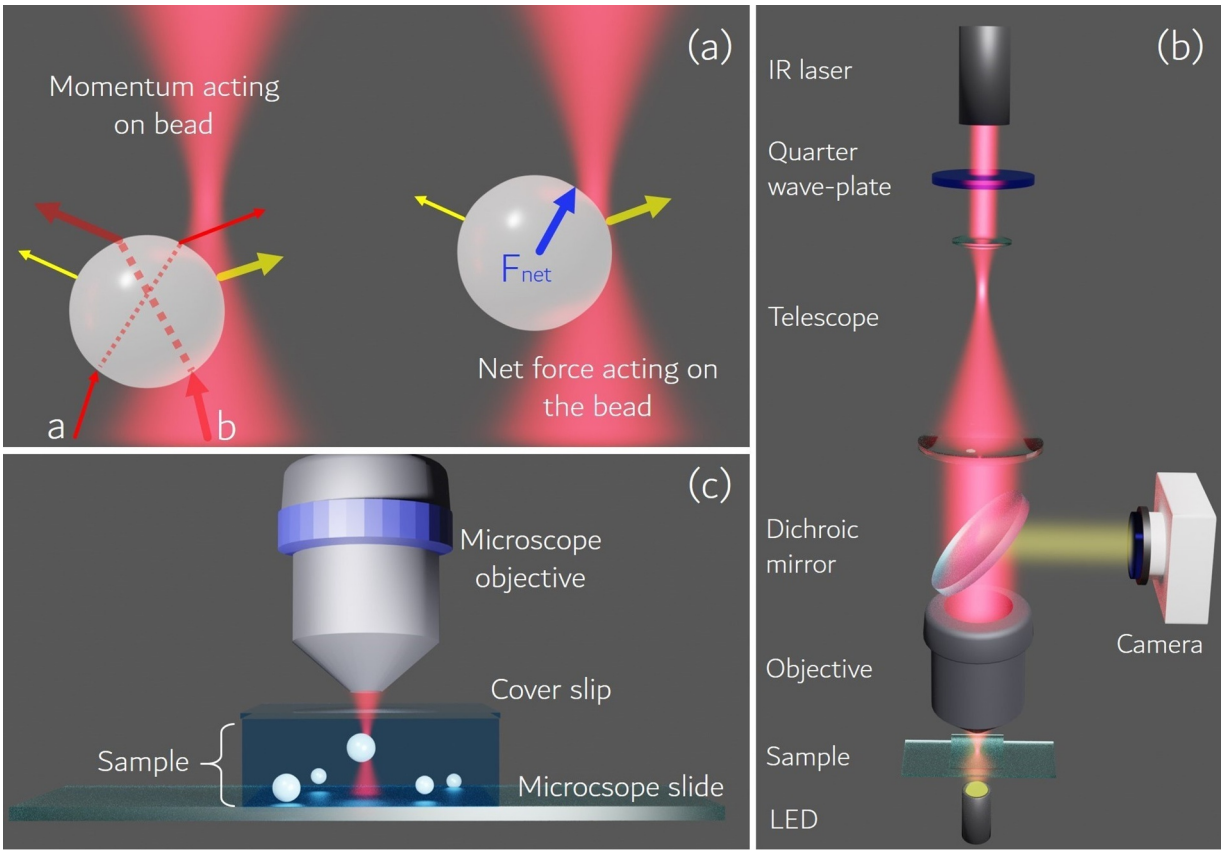

Fig. 2. (a) An intuitive representation of the trapping process in the Mie regime. The momentum (yellow arrows) of two rays *a* and *b* (red arrows) with different intensities propagating through a sphere is shown. The blue arrow indicates the restoring net force drawing the particle into the focal region. (b) Conventional OT setup schematic. The optical trap is formed inside a sample chamber with an objective with a high magnification and numerical aperture. The trapping process is imaged with a camera. (c) Model of the trapping process inside the sample chamber. (For interpretation of the references to color in this figure legend, the reader is referred to the web version of this article.)

focused Gaussian beam passing through the particle, one can observe the change in the beam propagation due to the difference in the refractive indices of the particle and the surrounding medium. A light ray at the central beam point is more intensive, which means that if the particle is shifted transversely from the focal spot, one side of the particle will refract more light away from the center of the trap than toward. The momentum carried by the light will be passed to the object, forming the net force, which, due to the total momentum conservation, is compensated for by the force pushing the particle toward the center of the trap. The equilibrium position of the object in the trap is reached by tight focusing using a lens with a high numerical aperture, which enables the dominance of the gradient force over scattering.

2) If the particle size is significantly smaller than the wavelength, $r << \lambda$, the polarizability of the object plays the decisive role. The particle is considered as an oscillating dipole in an electric field; hence, the Rayleigh limit [37] description based on wave optics laws must be applied for an adequate description. The particle is pulled toward the most intensive point of the beam, minimizing the particle energy. The force is independent of the object shape and changes the magnitude with the particle orientation. The scattering force pushes the particle in the direction of light propagation, while the gradient force draws it toward the brightest part of the beam. The stable trapping is established when the gradient force exceeds the scattering force. The competition between the two forces ensures stable trapping.

3) The third concept describes the case where the laser wavelength is comparable to the particle size, $r \approx \lambda$. This approach requires extensive mathematical treatment and still has not been implemented for an adequate description. The accurate modeling was implemented by applying Lorenz-Mie theory [38] to describe the scattering of a plane wave by a spherical particle of an arbitrary size, refractive index and wavelength. An optical force calculation for Gaussian and arbitrarily shaped beams requires the use of the generalized Lorenz-Mie scattering or T-matrix theory, which have been discussed elsewhere [39,40].

2.1. Optical tweezers configuration basics

A summary of the basic theory and construction of OT can be found in Ashkin [41] and [42]. Several configurations and extensions have been introduced for the conventional OT, which are defined by the specimen under study and the purposes of the researchers. Modifications and coupling with other methods, applied to the first implementation of OT [4], have significantly extended researchers' capabilities and led to the emergence of a variety of powerful instruments, such as holographic OT [32], speckle OT [43], Raman OT [44], optical stretchers [16], methods allowing particle rotation by transferring spin [45,46] and orbital angular momentum [47], etc. Comprehensive guides revealing how to build the simplest OT configuration can be found in Appleyard et al. [48], Firby et al. [49], as well as clarified instructions for more advanced versions of OT [50].

An OT system can be assembled around a commercially available microscope (preference is usually given to inverted models), which greatly simplifies the adjustment of the key parts [51,52]. The conventional OT setup consists of parts that can be adjusted to make (Fig. 2(b)) a household setup. However, powerful commercial OT are currently available, enabling fast and user-friendly accurate measurements of bimolecular interactions [53].

Optical tweezers are formed by a sharply focused laser beam, with the focal spot forming the tip of the tweezers, which can be used to pick and move objects. The typical range of forces imposed by the optical trap on the object is usually on the order of tens of piconewtons (pN). A brief overview of the key parts for assembling a conventional OT suitable for cell studies is given below.

1. **High-numerical-aperture microscope objective**. An objective is an essential part of OT, which provides stable three-dimensional trapping. Typically, these objectives have a high numerical aperture $NA \geq 1$ to ensure strong focusing and a high magnification of $100\times$ because a larger incident angle of the laser beam on the particle produces a stronger force. Refraction index matching is achieved by water or oil immersion. Depending on the OT type, the objective can be introduced into the optical scheme of the OT; in this case, all the parts require precise adjustment. The microscope-based OT bypass this problem, considerably simplifying the process of arrangement.
2. **Laser source.** The most convenient choice for biological samples is a 1064-nm diode-pumped Nd:YAG laser of a few hundred mW of power, since low absorption in the infrared range (therapeutic window) eliminates photodamage. The requirement for creating as small a focus as possible requires that the trapping laser source has a high degree of spatial coherence, such as a single-mode Gaussian laser. Significantly enhanced trapping has been achieved via structured scattering when specially structured incident light causes beamsplitter-like interactions with scattering particles [54].
3. **Lenses.** Lenses are introduced to a telescope to expand the beam (beam expander) for slight overfilling of the back aperture of the objective lens so that the beam can be focused to a diffraction limit.
4. **Trap positioning.** To perform movements of the trapping beam in the lateral plane, steering mirrors or acousto-optic deflectors are usually incorporated. An automated XYZ piezoelectric steerable stage instead provides sample translation in three dimensions [55].
5. **Sample imaging.** Sample imaging is implemented through backlight sample illumination and with a camera. The picture is seen on a computer screen. The quadrant photodiode (QPD) is the most widespread and reliable positioning system, offering object positioning by deflection of the laser beam. Large objects, for example, cells, can be imaged and tracked through a high-frame-rate camera [56].
6. **Sample chamber.** In the classic representation, a sample chamber consists of a microscope slide with an attached cover slip. The space in between is filled with a liquid sample (Fig. 2(c)).

Biological objects absorb light of the visible (380–740 nm) and infrared (IR) (1300–3000 nm) spectra due to their water content.

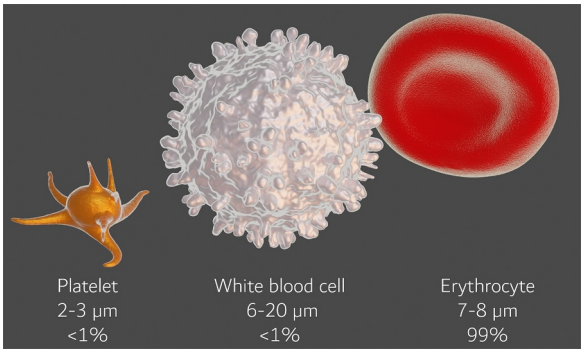

Fig. 3. Models of the main blood cell components: platelets, white blood cells and erythrocytes.

This property is the cause of the undesirable thermal effect [27], which can be avoided using near-infrared region (NIR) wavelengths within 700–1300 nm, where light can penetrate deeper into biological tissue. The medium can also minimize the heating caused by laser light through energy dissipation to the environment.

3. Blood components

Blood is a multicomponent substance with two major components: plasma (55%) a solution of organic molecules, proteins, and salts and formed elements, i.e., blood cells (45%). Formed components mainly include RBCs (99%), white blood cells (WBCs), leukocytes ($< 1\%$), and platelets ($< 1\%$) [57] (Fig. 3). The ratio of the main blood constituents is 1 leukocyte per 25 thrombocytes per 500 RBCs. Red blood cells and platelets are devoid of nuclei, while all WBCs have nuclei. WBCs appear in different forms defined by the unique function of the immune system to offer a protective response to infections, while RBCs perform mostly oxygen transfer.

Blood-based diagnostics has been well established in medical testing for a long time. Researchers still discover new evidence of the correlation of blood properties with pathological organism states, widening the informativity of conventional blood tests. The rheological properties of blood reflect the ability of red blood cells to be transported through blood vessels normally. In addition to hematocrit and plasma viscosity, an essential contribution to the blood flow properties is provided by cellular factors, mostly by the intrinsic mechanical properties of RBCs as the most abundant blood cell component. RBC deformability and aggregation have a pronounced effect on the blood flow in smaller blood vessels and in microcirculation. Despite their significantly lower blood count, the numbers of WBCs and platelets have been found to affect blood viscosity [58].

WBCs can be classified into five cell types: neutrophils, eosinophils, basophils, monocytes, and lymphocytes (T cells and B-cells), which all together offer protection against foreign substances. Neutrophils are the most abundant WBC type, constituting over 50% of the circulating leukocytes; thus, the majority of functions are provided by neutrophils. Leukocyte mechanical properties are manifested the most during the inflammatory response. The current paradigm for neutrophil recruitment is a multistep cascade of leukocyte adhesion conjugated with molecular stimulators. In general, after leaving a capillary, a leukocyte experiences margination by stream erythrocytes, which force the cell toward the venular endothelium [59]. This results in the leukocyte rolling through the weak adhesion to the endothelium, which becomes stronger after cell activation. After reaching stationary attachment, the leukocyte can migrate through the endothelium wall. Therefore, the deformability of WBCs is essential for rolling, resistance to blood flow, and adhesion, i.e. migration to the site of infection.

Being a multicomponent cell, a WBC is more complex than an RBC; its viscosity depends on its intracellular and membrane composition and its activation state when different mediators are involved [60]. Despite the majority of studies on WBCs being conducted with neutrophils, OT has become a powerful tool for lymphocyte studies.

Platelets are the first responders to injuries, accumulate at the site of injury, and, through a cascade of biochemical reactions, create a clot to stop bleeding. Among other blood cells, platelets are more sensitive to mechanical stress. Platelets have a high actin concentration and integrin density, which make them perfect for serving as mechanosensors. Applied force initiates the activation of intracellular elements, leading to shape change and fragmentation [61]. This dynamical change in mechanical properties limits the application of instruments to platelet stiffness measurements. The most suitable method is noncontactless, excludes cell adherence and exerts a limited shear flow, enabling the stiffness measurement of unactivated free-floating platelets. There are no OT studies that meet these requirements, though some studies were conducted to investigate integrin-fibrinogen binding (Section *OT applications for WBCs and platelets*).

3.1. RBC mechanical properties

RBC deformability is the combined result of several mechanical and geometrical properties of RBCs. Factors such as the internal viscosity and surface area-to-volume ratio of the cells as well as membrane elasticity and viscosity are determinants of the overall deformability of RBCs. RBCs are commonly used as model systems for cellular biomechanics studies due to their relative morphological simplicity and availability. The application of OT in RBC studies has led to many important findings in hemorheology [62].

A healthy erythrocyte has a biconcave discoid geometry with a diameter of 6–8 μm and a thickness at the center of 0.8–1 μm, with a slight thickening at the periphery to 2–2.5 μm. The RBC biomechanical properties are dictated by the RBC structure. The plasma membrane of an RBC comprises a phospholipid bilayer supported by an underlying hexagonal lattice of spectrin and actin, which regulates the discotic shape stability and elasticity. Since the inner cell composition of RBCs is essentially a viscous fluid, the elastic membrane is mainly responsible for the stress resistance. There are three main structure-related factors contributing to RBC deformation [63]:

1. A high surface-area-to-volume ratio $S/V \sim 1.5$ [64], which enables the highly flexible RBC structure. This explains the ability of RBCs to squeeze through the narrowest capillaries (< 3 μm diameter) and even through the sieves in the spleen (1 μm openings) [65]. The shape of an RBC is easily affected by the shear flow and walls of the microvessels, deforming it to a "bullet" -like shape, but immediately after these pressure effects are released, the cell recovers to its original shape. In contrast, a decrease in the S/V parameter is associated with the higher RBC stiffness observed for common RBC disorders such as malaria, hemolytic anemia, and hereditary spherocytosis [66].
2. Cytoplasmic viscosity is governed by the presence of hemoglobin, which provides fast RBC shape changes in response to fluid shear stress.
3. The viscoelastic properties of RBCs are defined by the properties of the cell membrane layered structure: 1) the skeleton underlying the protein network, 2) the lipid bilayer, and 3) the outer carbohydrate-rich glycocalyx [63]. Mechanical properties in general describe how a cell would react to applied stress. The deformations of solid materials are dictated by Young's modulus (E) or the elasticity, with units of pascals [Pa]), while for fluids, it is defined by the viscosity [Pa s]. The viscosity of the membrane η [μNs/m] is the rate of its deformation. Young's modulus is defined by the ratio between the stress and the strain along a certain axis. Cells are intrinsically viscoelastic because they possess both deformation and an elastic response to deformation [67]. Therefore, the rheological properties of the RBC membrane are defined by its mechanical coefficients and three elastic and viscous moduli [68]:

- The elastic energy storage upon elongation or shear deformation of the RBC membrane is represented by the shear elastic modulus μ [μN/m]. The shear modulus of RBCs has been found to be in the range of 2.5–10 μN/m [69].
- The bending modulus (stiffness) B [N/m] characterizes the bilipid layer of the RBC membrane associated with resting shape changes, without shear or expansion [70]. The bending modulus is considered to be too small to impact the membrane response [71] and is usually 1.8×10^{-12} μN/m.
- The area compressibility or expansion modulus K [72] is the resistance to area compression or extension. This parameter is dependent on the total number of lipids in the membrane and is usually in the range of 3–6 $\times 10^5$ μN/m. The relation between these parameter values means that RBCs bend easily, shearing is difficult to achieve and RBC compression is the most challenging to accomplish.

Blood behaves as a non-Newtonian fluid: the viscosity of blood varies with the shear rate. RBC deformability largely determines the blood viscosity parameters under high shear stress, while RBC aggregation contributes to low shear stress conditions. There is solid evidence that RBC deformability impairment correlates with pathological alternations [73,74]. This interplay is of high clinical interest and has been revealed for a number of diseases: diabetes [75], obesity [76], malaria [77], sickle cell anemia [78], cardiovascular diseases [79], chronic renal failure [80], arterial stiffness [81], and hereditary disorders [82].

3.2. RBC aggregation

RBC aggregation is a reversible process of RBC clumping in linear (rouleaux) and then three-dimensional structures, as shown in Fig. 4(a). Blood viscosity is inversely proportional to the shear stress. RBC aggregates are formed under static or low-shear conditions

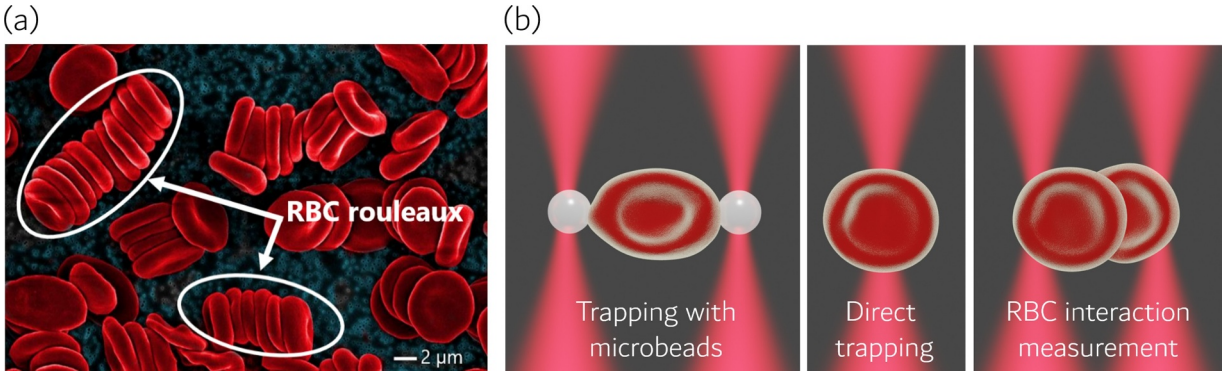

Fig. 4. (a) Scanning electron microscopy (SEM) colored images of RBC aggregates (rouleaux). (b) Schematics of RBC trapping approaches: trapping with microbeads attached to RBCs, direct RBC trapping, and RBC interaction measurement.

and disrupted with increasing shear rate. The blood composition and the functional properties of macromolecules, particularly blood plasma proteins, affect the RBC aggregation [83]. Therefore, the level of RBC aggregation in standard hematological blood tests is estimated by the erythrocyte sedimentation rate (ESR) for the rough assessment of inflammatory risks.

The RBC membrane fluid lipid bilayer, in addition to phospholipids, includes glycolipids and cholesterols, with embedded or attached proteins and glycoproteins. Negatively charged sialylated glycolipids in the RBC membrane result in electrostatic repulsion between RBCs, creating an electric zeta potential (ζ) [84]. In other words, the zeta potential represents the RBC surface charge, which prevents RBC aggregation [85]. In blood plasma, the negative RBC surface is surrounded by cations, with the following diffuse layer of cations and anions in a mixture. A more detailed description of RBC deformability and aggregation measurements with OT is addressed later in this paper.

3.3. General experimental guides for RBC optical trapping

The typical experimental routine for the optical trapping of RBCs starts with blood withdrawal. The advantage of OT is the small sample volume needed for experiments; usually approximately 20 μm is enough for one series of experiments. Blood is obtained by the finger-prick method from a donor prior to experimentation or can be acquired from a blood bank. RBCs from the blood sample (hematocrit 45%) are washed with phosphate buffered saline (PBS, pH 7.4) by centrifugation. Sedimented RBCs are then accurately taken from a vial bottom and suspended in a desirable buffer and at the required concentration, which has to be low enough to provide single-cell trapping. The sample is placed in a special chamber, usually made of a glass slide with a glass coverslip attached to a double-sided tape to form a gap in which to place the sample. It is highly advised to seal the open edges of this cuvette with Vaseline to prevent drying of the sample and thermal drift, which will interfere with the measurements.

Many experiments have been performed in phosphate buffer saline (PBS) as a host medium, isotonic to blood plasma. RBCs in vivo are suspended in plasma containing electrolytes, albumin, fibrinogen and other macromolecules, while PBS is just a water-based salt solution. To mimic the natural surroundings of RBCs, an autologous plasma is preferable to preserve the natural biconcave RBC shape [86]. Normally, the relative viscosity values of whole blood and plasma are approximately 4–5 and 1.8 mPa s, respectively [87]. The difference between the PBS and plasma viscosities have to be taken into consideration for optical trapping calibration either by the drag force method or with a QPD.

Foo et al. [88] studied the effect of heating and cooling on the elastic properties of individual RBCs based on the temperature correlation with the mechanical properties of RBCs [89]. RBC deformation under hydrodynamic flow at body temperature (36 ˚C) significantly exceeded the deformation reachable at room temperature (25 ˚C). The irreversible changes were caused by heating of the cells from 23 to 42 ˚C and cooling back to 23 ˚C, which made the RBCs much softer compared to their initial elasticity. This study clearly demonstrated the importance of temperature control in single-cell studies.

Typically, RBCs can be trapped either directly or using specific handles, such as microspheres attached to the cell surface through specific or nonspecific binding (Fig. 4(b)). Trapping efficiency depends on the difference between the refraction index of an RBC and the surrounding liquid. An RBC behaves as a lens, being an almost transparent asymmetric dielectric object for NIR light, having a spatially uniform refractive index as the cell lacks a nucleus and the majority of organelles [90]. Compared to blood plasma and buffer solutions, RBCs in general have a higher refractive index, resulting in effective optical trapping and manipulation.

4. Intrinsic RBC deformation properties studied with OT

The first experiment demonstrating the feasibility of OT usage for RBC trapping was performed by Ashkin [5]. The classical installation based on a conventional microscope was equipped with a 1064-nm Nd-YAG laser. Damage-free trapping was performed over a range of powers (4–40 mW) with no changes in the RBC flexibility observed. The latter decreased only after keeping the RBCs at increased power (80 mW) for tens of minutes. This experiment paved the way toward RBC optical trapping. A more recent study [91], however, demonstrated that optical trapping at 10 mW for 2 min caused a decrease in RBC cell elasticity, which was greater at shorter NIR wavelengths.

Experimental observation of RBCs upon trapping with a single beam has shown that an RBC orients itself with a maximum diameter along the direction of beam propagation, enclosing the maximum energy [17]. Despite fruitful experimental works, a theoretical description was lacking for a long time, arising almost 10 years after the first RBC trapping [92]. RBCs possess a discotic shape and are subject to strong shape deformations, making a theoretical description of RBC behavior in response to OT far from trivial. Simple analytical calculations given for spheres are not applicable. Grover et al. [92] considered an RBC trapped in dual-beam OT and traced the rays passing through the cell, enabling calculation of the scattering and gradient forces. The torque, which induces object alignment in OT, was presented as a function of RBC position at different angles. An RBC reaches the equilibrium orientation at 180˚, parallel to the beam spreading direction, whereas an unstable equilibrium corresponds to 90˚ (Fig. 5(a). Later on, this observation was proved using confocal fluorescence microscopy [93]. However, in the study by Ghosh et al. [94], RBCs were claimed to be folded in a rod-like shape under optical forces, and a model, based on the concept of buckling instabilities, was offered to describe this phenomenon.

An RBC was trapped with multiple OT [86]: two traps at the RBC edges and a third one, in the middle, that was shifted, causing the cell shape distortion. Registering the relaxation time of the RBC shape recovery immediately after turning off the traps demonstrated that young RBCs recovered almost twice as fast (162 ms) as old cells (353 ms). In addition, a remarkable difference in the recovery time was found between RBCs in a buffer solution and in blood plasma, suggesting plasma as a natural habitat that is a preferable medium to model in vivo conditions.

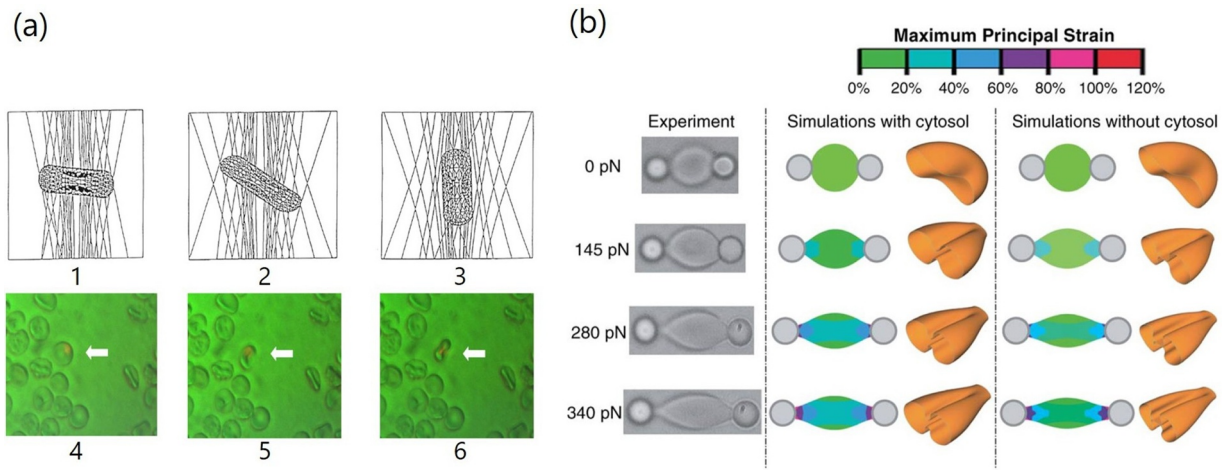

Fig. 5. (a) Theoretical modeling (top) and corresponding experimental results (bottom row): (a, d) erythrocyte before trapping, (b, e) during reorientation in a dual-beam optical trap, and (c, f) after stable trapping is achieved. Figures in the top row demonstrate triangular elements used in the algorithm for the theoretical determination of behavior. Adapted with permission from [92]. The Optical Society. (b) Two silica microbeads diametrically attached to an RBC: one of them is attached to the glass surface, while the second one is trapped by the OT. Second column shows a simulation of the stretched biconcave cell undergoing large deformation under forces from 0 to 340 pN with cytosol, and the third column, without cytosol. The color contours represent the spatial variation of the constant maximum principal strain [97].

The RBC membrane mechanics is mainly determined by the cellular cytoskeleton - a complex network of interlinked proteins, filaments, microtubules and linkers. To retrieve specific information, OT were applied to study an isolated RBC membrane skeleton [95]. Trapped silica beads coupled with an RBC were subjected to the stream flow of detergent, which washes out the membrane and intracellular structures, leaving only the membrane skeleton. The cytoskeleton network under this treatment became nearly spherical and flexible. The flow chamber allowed exposing different media on the trapped skeleton and performing observations under different conditions.

The shear modulus was inferred from measurements of the elastic coefficients of RBCs in an experimental implementation by Henon et al. [18], where two silica beads were used as handles to stretch the RBCs. By moving one of the handles away, a resultant force of 60 pN (P $\approx$ 400 mW) was developed. The applied forces caused RBC shape distortion, which was presented as a change in diameter versus the applied force. The shear moduli $\mu = 2.5 \pm 0.4$ μN/m for both discotic and nearly spherical swollen cells were extracted from the slope of the linear part of this dependency.

A similar experimental approach but with clinical emphasis to elucidate the role of hemolytic disorders with RBC elasticity was conducted by Sleep et al. [96]. The shear modulus at 15 pN of force was derived to be 200 μN/m for an unmodified cell ghost and for modified cells by chymotrypsin, PCMS and NEM. The suggested reason for this discrepancy of the shear modulus value compared to the data of Sleep et al. was that the bending modulus was accounted for, whereas Henon et al. neglected its impact.

The abovementioned approaches, however, could induce a deformation of only 15% of the original cell size due to the small forces applied to the handles. Knowing that RBCs in natural in vivo conditions undergo much higher deformations, researchers have sought for a way to allow higher force loads on cells.

In the study by Dao et al. [97], the authors succeeded in increasing the force load up to 400 pN by using larger microbeads, which, at the same time, minimized heating of the cell. Three-dimensional finite element analysis for a biconcave RBC has been applied to extract the elastic properties of the cell membrane, upon varying geometry, cytosol properties and contact-dependent loading force of the attached beads (Fig. 5(b)), which were confirmed to contribute to the deformation response of the cell. The values of the membrane shear modulus were found to be in the range of 11–18 μN/m, while a bending modulus of $1 - 9 \times 10^{19}$ Nm was considered insignificant in the overall deformation. This later led to the clinical application of OT to investigate malaria-infected cells [98]. The rigidity of malaria-infected RBCs is associated with a capillary blockage leading to organ failure. Therefore, OT have become an excellent tool for the diagnosis of malaria (more details are given in Section *RBC deformability in diseased states: clinical implications*).

5. Optical stretcher

The exertion of extreme pressure on RBCs was eventually achieved with the optical stretcher (OS) introduced by Guck et al. [99,100], which has been largely applied in cell studies [16]. Combined with an optofluidic device, the OS performs fast measurements of elasticity of the whole cell. An OS exploits the phenomena that occur when a cell is trapped between two identical counterpropagating divergent laser beams with a Gaussian intensity profile. A cell experiencing total momentum transfer on its surface is stretched along the axis of beam propagation instead of undergoing the intuitively expected compression. A schematic representation of a trapped RBC in an optical stretcher is shown in Fig. 6(a).

The first prototype was a simple flow chamber filled with an RBC suspension and two optical fibers inserted perpendicular to the

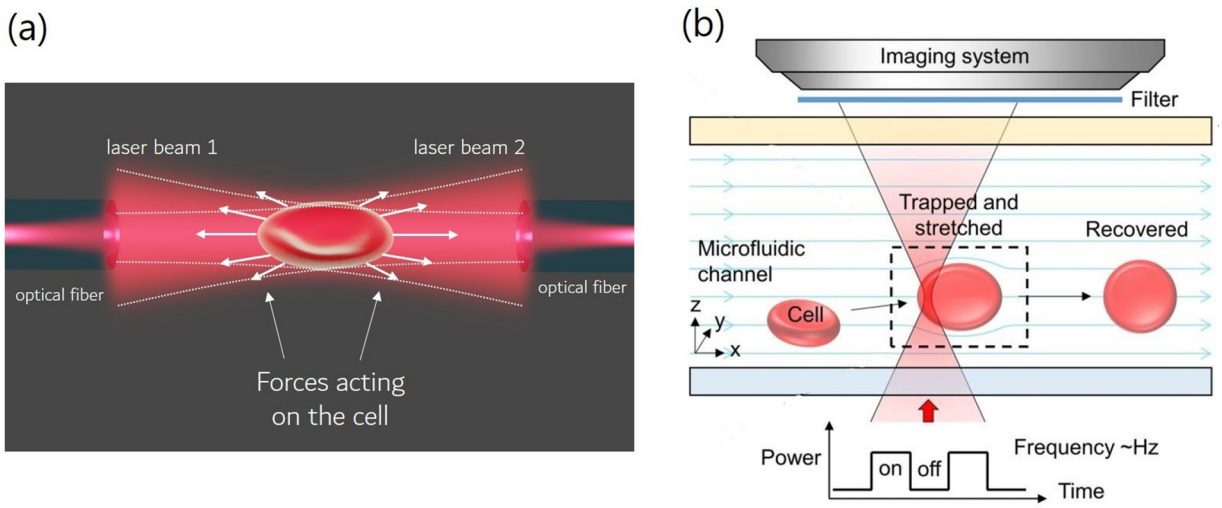

Fig. 6. (a) Schematic representation of an RBC trapped in the middle of two opposing lasers 1 and 2, forming an optical stretcher. (b) The principle of the optofluidic "tweeze-and-drag" cell stretcher. The RBC is trapped by a periodically chopped laser inside the microfluidic channel, stretched by the flow and then released. Reproduced from [24].

flow. The measurement of elasticity was optimized by repeating the same steps: after RBC trapping, the flow is stopped, a measurement is taken and the trapped cell is released [101]. A tunable Ti-Sapphire laser (wavelength of 780 nm) was used for trapping to strike a balance between decreased protein (UV range) and the water absorption (near-IR) of light to minimize the thermal effects. Indeed, RBCs trapped at intensities up to 300 mW are restored to their initial shapes, being indistinguishable from intact cells. The experiment was also conducted on swollen spherical RBCs. The peak stress along the beam axis was derived from the total power in each beam and cell deformation. RBC deformation followed the linear response to the applied laser power up to 350 mW ($\sigma_0 = 2$ N/m^2), with a relative deformation of 10%. Applying the membrane theory in this regime, at the chosen peak stress of 1.47 N/m^2, Guck et al. [101] derived the homogeneous Young's modulus $Eh = 39 \pm 14$ μN/m (where (h is the thickness of the cell membrane) and the corresponding shear modulus $\mu = 13 \pm 5$ μN/m. However, the theory did not fit the nonlinear behavior under higher peak stresses. At the peak $\sigma_0 = 2.55 \pm 0.1$ N/m^2 along the beam axis, the cell achieved an elongation of over 80%. This extreme corresponded to a 500 mW laser power or 400 pN force. Further peak stress exceeding $\sigma_0 = 3$ N/m^2 led to cell rupture.

It is interesting to note that cell softening occurred in the nonlinear regime, when the light imposed $\sigma_0 \geq 3$ N/m^2. The speculative explanation was that stress causes the membrane rearrangements to adapt to the load, resulting in higher stiffness. However, higher stress induces cytoskeleton rupture and RBC softening.

The newly emerged method requiring a precise mathematical description of the deformation behavior of RBCs in an OS is envisaged to be applied for analysis and transfer to cell diagnostics. Many studies made an effort to elaborate mathematical models for the original Guck experiment to achieve a more precise retrieval of the RBC deformation characteristics. Guck et al. [101] used the ray-optics model, and Bareil et al. [102,103] extended the model and provided more detailed information about the exact stress distribution on the spherical RBC surface in an OS $Eh = 20 \pm 2$ μN/m. In [104], previous data based on the cosine-squared approximation were compared with data obtained with the new ray-optics model, accounting for the focusing by the spherical interface, the actual experimental configuration, and the effects of multiple internal reflections, which were supposed to influence the cellular elasticity parameters. The calculated cell stiffness ($Eh = 54$ μN/m) was in excellent agreement with the experimental results, confirming the validity of the new numerical approach.

After retrieval of the optimal values of the membrane properties, the model was adjusted to the experimental values obtained by Guck (2000, 2001) [105]. The average shear stiffness was found to be approximately 4.611 μN/m for the nondimensional ratio of the shear modulus to the bending modulus, ranging from 10 to 300. Another mechanical model developed to calculate the RBC dynamic deformation showed great correlation with previous studies by Guck et al. [101] and Bareli et al. [103], giving area compressibility moduli $k = 0.56$ and 0.42 N/m and shear moduli $\mu = 9.5$ and 7.2 μN/m, respectively.

OT integration with microfluidics is one of the approaches to accelerate data acquisition. Sraj et al. [22,23] introduced a single-beam OS, applying laser diode bar in a microfluidic channel for RBC optical stretching as a high-throughput method for cell deformation cytometry. This method was proved feasible, as it provided shear modulus values comparable to those previously obtained.

A recent study by Yao at al. [24] demonstrated the advantages of combining an OS with a microfluidic channel. In this configuration, rabbit RBCs could be stretched in a microfluidic flow (2.5 μm/hour) by a periodically chopped laser beam, allowing for considerable acceleration of the mechanical characterization (1 cell/s). The concept is shown in Fig. 6(b).

6. RBC Deformability in diseased states: Clinical implications

The application of OT to detect the difference between healthy and pathological cells resulted in fruitful findings, which can be

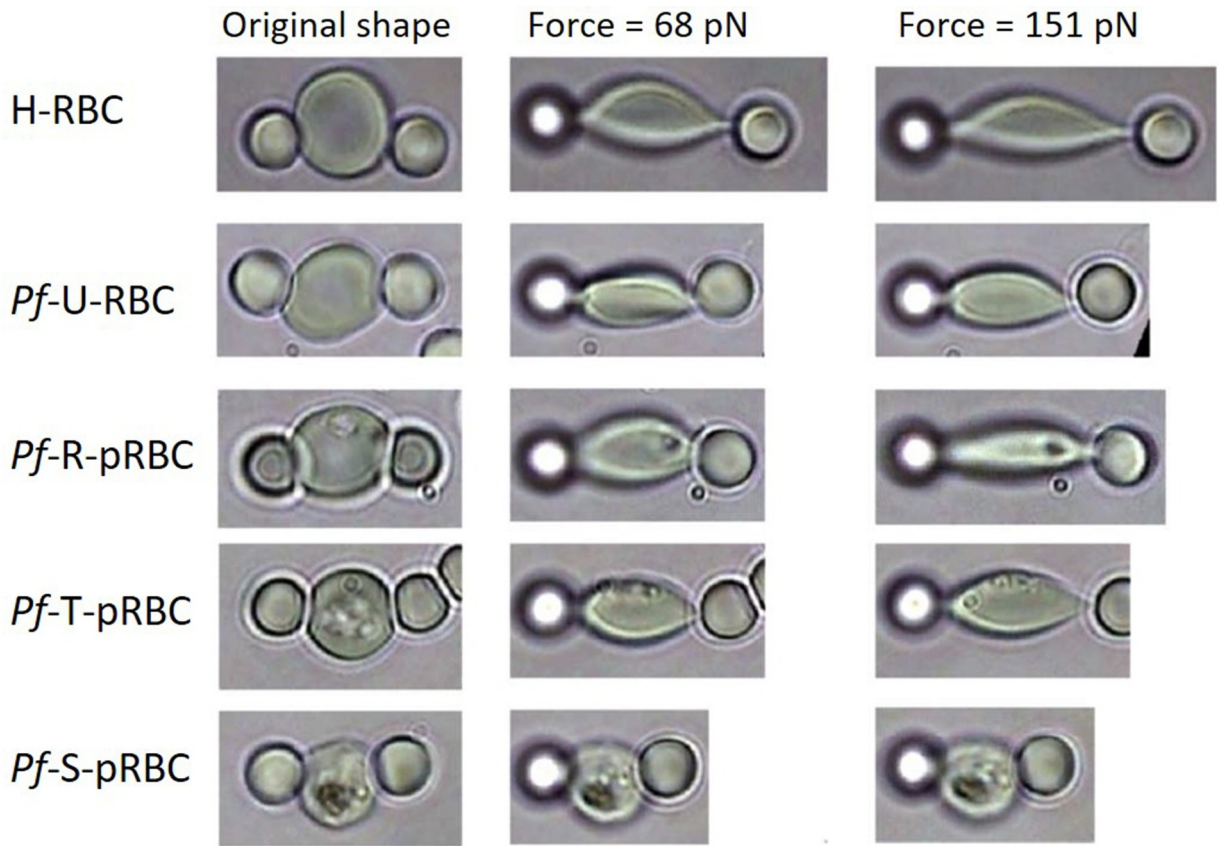

Fig. 7. Optical images of OT stretching of a healthy H-RBC, and different stages of malaria-infected cells, i.e., Pf-U-RBC (control uninfected), Pf-R-pRBC (early-stage infected), Pf-T-pRBC (mid-stage infected) and Pf-S-pRBC (late-stage infected), in a PBS solution at 25 °C: prior to tensile stretching by optical tweezers (left column), at a constant force of 68 ± 12 pN (middle column) and at a constant force of 151 ± 20 pN (right column). Reproduced from [98].

applied to clinical diagnostics. Micropipette aspiration experiments demonstrated the loss of deformability and abnormal circulatory behavior of infected RBCs [106]; therefore, more sensitive OT were widely applied to retrieve the properties of RBCs in pathological states.

In the experiment by Suresh et al. [107], one bead attached to an RBC was trapped, while a bead on the other side of the cell was attached to a glass plate. Applying forces up to 150 pN with an OS, a shear modulus increase was observed compared to that of healthy RBCs (H-RBCs) (5.3 μN/m) for malaria-infected RBCs at different developmental stages to values of 16, 21.3 and 53.3 μN/m for the ring (Pf-R-pRBC), trophozoite (Pf-T-pRBC) and schizonte (Pf-S-pRBC) stages, respectively. The Pf-U-RBC (exposed to the parasite but not infected), Pf-R-pRBC, Pf-T-pRBC and Pf-S-pRBC were, respectively, 1.5-, 3.0-, 4.0- and 10-fold more rigid than the H-RBC, indicating the linear loss of deformability during disease progression (Fig. 7).

Another approach by Mohanty et al. [108] revealed the distinct difference between malaria-infected and healthy RBCs. Healthy RBCs, while trapped in a hypertonic buffer, were rotated with linearly polarized light as a naturally occurring microrotor. Infected cells, in contrast, did not rotate in the field of the laser or showed much slower rotation speeds. The mechanism of RBC rotation in a hypertonic buffer was explained through the RBC shape change as a response to the structural asymmetric meniscus, which led to an uneven force distribution resulting in rotational torque that forced RBC rotation around the trap beam axis [109]. The same group later [110] investigated healthy and infected RBCs by applying viscous drag to stretch-trapped RBCs. The viscoelastic parameters retrieved from the measurements demonstrated the increased stiffness of malaria-parasite-infected cells. These cells were hardly deformable ($\mu = 13.5 \pm 5.3$), while healthy RBCs ($\mu = 4.97 \pm 1.6$) were deformed by weak viscous drag.

Byun et al. [111] demonstrated that sickle cell disease, associated with a defect in the hemoglobin structure, leading to RBC structure and deformability malfunctions, is the reason for rheology blood violation in patients.

The RBC response to a drug was analyzed in terms of the overall elasticity [112]. The data showed that RBCs from patients with sickle cell disease (HbSS patients) are less deformable than those in the control group, but no significant difference was found between HbSS and sickle cell trait (HbAS) patients. However, HbSS patients treated with hydroxyurea (HbSS/HU) for at least six months presented RBC deformability similar to that of the control group. The same method was applied to estimate the overall elasticity of RBCs from iron-deficient subjects and compare them to healthy donors [113]. The increased stiffness of RBCs from iron-deficient patients was associated with hemoglobin content rather than with the cell geometry or volume.

The effect of doxorubicin - a common drug in anticancer therapy - on the mechanics of DNA, leukemic blast cells and RBCs was also studied with OT by stretching the cells with 4.5 μm beads attached at opposite sides of a cell [114]. It was shown that doxorubicin increased the cell elasticity of leukemic blast cells, as well as of healthy RBCs, where the stiffness decreased twice from 15 ± 4 to 32 ± 3, which was explained by the high toxicity of the drug. Confocal laser scanning microscopy confirmed the incorporation of the drug into the RBC membrane and the distribution of doxorubicin over the cell volume.

Lima et al. [115] offered a method for comparing the viscoelastic properties of normal HbA and -thalassemia intermedia (Hb) RBCs with OT, with an additional estimation of the RBC negative charge by attaching cationic quantum dots. The study revealed an decrease in RBC elasticity and a reduction in the membrane charge for pathological cells.

OT were used to compare the deformability of healthy RBCs with cells obtained from patients with diabetic retinopathy (DR) and type 2 diabetes mellitus (DM) [116]. By RBC stretching, the authors analyzed the deformability index $DI = (I_{max} - I_0)/I_0$, where I_{max} is the final stretched length and I_0 the initial length. The index for DR RBCs (0.0635 ± 0.028) was smaller than that for DM RBCs (0.0645 ± 0.038) and control RBCs (0.0698 ± 0.0224), indicating that the DR erythrocytes are less deformable and more swollen when compared to DM RBCs. They also noted the different initial sizes I_0, which was higher for DR RBCs and DM cells than for the control and associated with the reduced cell deformability.

Blood transfusion efficacy was estimated in patients with sickle cell anemia (SCA) [117]. By trapping RBCs at different powers and then releasing them, the maximum and minimum diameters and relaxation time were analyzed. Both parameters were lower in the case of SCA cells.

7. Mutual RBC interactions

The OT technique can serve as an accurate and fast methodology for revealing the response of RBCs in terms of the membrane mechanical properties, providing precise quantitative information about the interaction forces between studied cells. In addition to the elastic properties of RBCs, the most important blood property is RBC aggregation. RBC aggregation is a reversible process of RBC clumping in linear (rouleaux) and then three-dimensional structures [118]. Viscosity is inversely proportional to the shear stress when RBC aggregates are formed under static or low-shear conditions and is disrupted with increasing shear rate. RBC aggregation is dependent on the plasma protein composition and membrane surface proteins. For example, aggregation increase is peculiar to inflammatory disorders [119]. Surprisingly, the exact mechanism of RBC interaction is still unknown. However, it was found to vary under a number of clinical conditions (infections, cardiovascular and hematological diseases, and metabolic disorders), therefore holding the key to understanding many diseases and finding ways to effectively cure them. Two coexisting and contradictory models of the process are bridging [120] and depletion [121]. Earlier experiments showed results in favor of both theories, leaving the dilemma unresolved.

The first RBC-induced interaction was carried out with double-beam OT in 1997 [122]. The work focused on the disaggregation of two trapped cells. The cells forming a doublet were pulled apart. Measurements in plasma showed that the force needed to form an aggregate is negligible, while sliding RBCs apart required much higher force and resulted in the formation of a tether between the cells. Observations favored the cross-bridging model of interactions. It is worth noting that RBC binding does not occur in phosphate buffer saline but in plasma and solutions of polymers, proteins or dextran.

In [123], researchers measured the aggregation parameters of normal and pathological RBCs affected by systemic lupus erythematosus (SLE), an autoimmune disease resulting, in addition to other syndromes, in enhanced RBC agglutination. Using dual-beam OT, they pulled RBCs in a rouleax, registering the achievable displacement. The aggregation force and speed values were almost two times higher for SLE RBCs than for normal cells. The studies by K. Lee et al. were aimed at retrieving the effects influencing RBC aggregation, such as temperature [124] and protein composition [125], and to find a preferable model of RBC interactions.

It was shown in Lee et al. [126] that by measuring the forces between interacting RBCs with double-channel OT, the aggregation and disaggregation forces significantly differ, as the force applied to separate cells was much higher. The RBC aggregation process was described with the depletion model, while disaggregation was assumed to be associated with cross-bridges formation, as the dynamics of the process demonstrate an increase in force upon cell separation. A recent study [127] that combined OT with microfluidic and fluorescence microscopy revealed that 70 kDa dextran adsorption on the RBC surface affects its deformability. OT supplemented with SEM imaging (Fig. 8(a–c)) were applied to study RBC interactions in blood plasma and in a polymer dextran solution to reveal the model of RBC aggregation. Despite the different types of mutual interactions in plasma and uniform-sized dextran, a mixture of dextrans with molecular weights and concentration ratios similar to those of proteins in blood plasma can serve as a plasma model, resulting in a similar interaction energy dependence. Based on the results, the authors [128] suggested that the most probable mechanism of RBC interaction includes both depletion and bridging mechanisms, depending on the environment of the studied RBCs, and that a hybrid model utilizing the mechanisms of cross-bridges and depletion should be considered. The same interaction model was observed in subsequent studies by Avsievich et al. [129], who demonstrated that nanocapsules do not influence RBC interactions, and Zhu et al., who revealed the influence of continuous and pulsed laser irradiation on RBC aggregation [130].

Another methodology for testing new synthetic materials and healthcare pharmaceutical products in terms of their potential applicability was proposed in Avsievich et al. [131]. Mutual RBC interactions were estimated with OT upon treatment with different nanoparticles (NPs). NP-induced aggregation was also estimated by conventional optical microscopy. The nanodiamonds used in the study induced cell damaging, which resulted in stronger interaction forces between RBCs (Fig. 8(d)). In the future, the method can be used as the first step of NP validation for biomedical purposes.

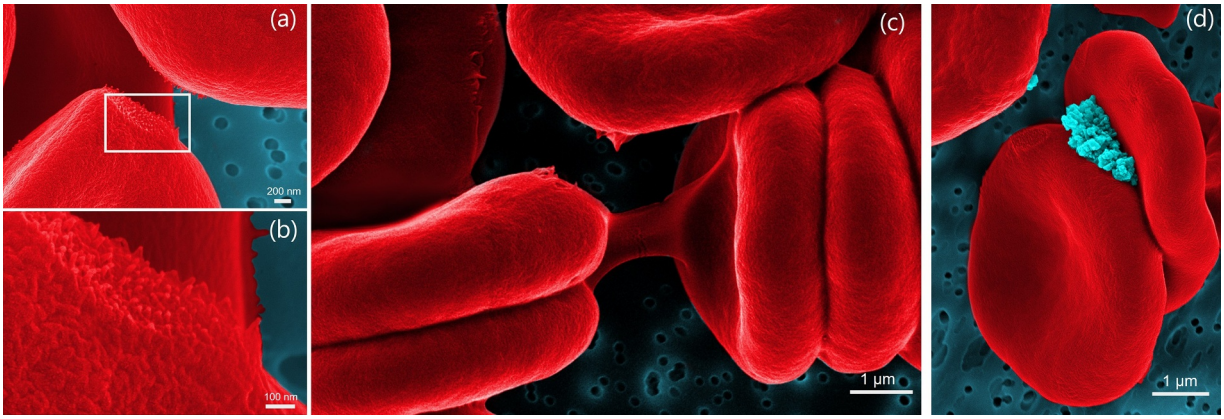

Fig. 8. Colored SEM images of separated RBCs. (a) The white rectangle indicates an enlarged area on the cell surface with cilia at the RBC membrane, which is shown in (b) for blood plasma and in (c) for a 500 kDa dextran solution. Reprinted with permission from [128]. The Optical Society. (d) Nanodiamond-induced RBC aggregation [131].

RBC aggregation was studied in a serum in the presence of solutions used for hemagglutination tests: erythrocyte antibodies and associated agglutination potentiator solutions (dextran, low ionic strength solutions [LISSs] and enzymes) [132]. An RBC rouleau was attached to a trapped silica bead, while the other trap was used to pull cells apart. Retrieved from the measurements, the force and the apparent membrane viscosity values were in accordance with the immunohematological routine.

In the study of RBC coagulation [133], the minimal force between coagulated RBCs was registered. Three main coagulation phases were found. First, RBCs were randomly distributed; next, they slowly started to vibrate around their equilibrium positions; and then, they moved slowly toward the coagulated group. In the final phase, the RBCs moved quickly until completing the process by merging with the coagulate. Treatment with heparin extended the first phase of the coagulation, while tranexamic acid induced the RBCs to quickly coagulate in the third stage.

8. Optical rotation and orientation (optical spanners)

The first RBC rotation was achieved by S. Sato in 1991 [17]. Instead of the TEM_{00} mode of the trapping beam, the higher-order modes of a Nd-YAG laser beam were applied for trapping. The force generated by a TEM_{01} beam was 20% higher than that of the standard TEM_{00} mode, having a larger incident angle at the periphery on the object, which resulted in higher refraction and, consequently, stronger trapping. Upon trapping the RBC with TEM_{0n}, which produced a nonuniform intensity distribution, the cell was oriented along the elongated beam intensity distribution. The rotation of the cell was achieved by beam rotation. A simpler and more efficient approach was demonstrated by Dasgupta et al. [134]. The controlled rotation was implemented by using cylindrical lenses, which generate an elliptic beam profile (line tweezers).

However, the method was still limited by object rotation around an axis, therefore making it inapplicable in microscopy. The optical rotator offered by Kreysing et al. [135] was based on a dual-beam fiber trap where one of the fibers is asymmetric; in this configuration, cells, being optically anisotropic, follow this rotation of beam asymmetry and can be oriented at different angles (Fig. 9(a)). This approach allowing cell orientation and rotation perpendicular to the optical axis of a light microscope offers the advantage of isotropic resolution for tomographic microscopy applications. In 2014, the same group [136] improved the previous approach using beams with high modal purity, which are well defined in three dimensions. Fibers integrated in a lab-on-chip system were used to carry out the rotational manipulation of RBCs (Fig. 9(b)).

The change in RBC orientation has been demonstrated, which is especially important for keeping a cell in a desirable orientation, for example, in the Raman spectroscopy measurements conducted by Dasgupta et al. [137]. Using the annular intensity profile of the Laguerre-Gaussian trapping beam modes, which increases with the topological charge of the mode, control over the RBC orientation in a vertical plane was achieved. Moreover, this trap transferred the orbital angular momentum to the RBC, forcing its rotation in an isotonic solution. Fiber probes were shown to not only rotate but also deform RBCs [138]. Two tapered fiber-optic probes (TFPs) with a laser beam of 980-nm wavelength can stably trap a cell by adjusting the TFP position and magnitude. The trapped RBC can be rotated around different axes (Fig. 9(c)).

The net angular momentum of laser beams includes the spin [139] and orbital angular momentum [140]. The spin or orbital momentum is transferred to the object, causing spinning of the object or orbital rotation. RBC spin and orbital rotation were observed by offsetting the trapping fibers transversely [141]. Upon increasing the offsetting distance between the fibers, the RBC spinning transitions to orbital rotation, moving along the elliptic orbit. Within the translation from spinning to orbital rotation, the RBC still spins, decreasing the frequency with the offset distance.

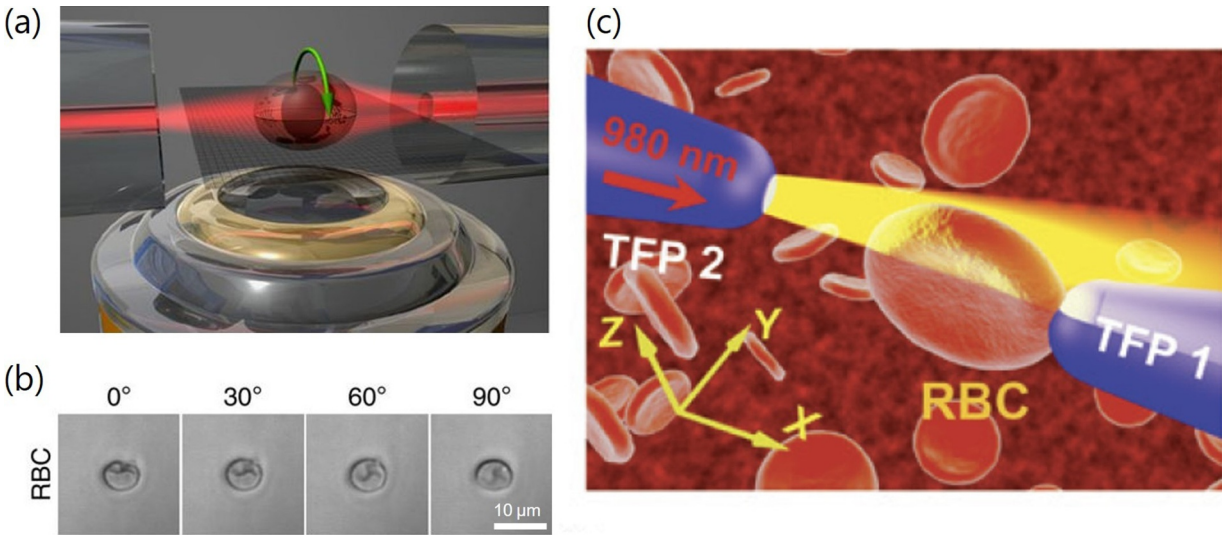

Fig. 9. (a) Schematic illustrating the basic setup of the optical spanner. Two opposing, coaxially aligned optical fibers emit a near-Gaussian beam (single-mode fiber, from left) and a rotational orientation-enforcing LP11-type beam (few-mode fiber, from right). (b) Image sequence showing the precise orientation of an RBC between 0° and 90°. Reproduced from [136]. (c) Schematics of RBC rotation around the *x*-axis [138].

9. Use of Raman trapping spectroscopy to reveal the living cell chemical composition

The combination of OT with Raman spectroscopy significantly improved the Raman spectroscopy of living cells. The OT technique became highly appreciated for the immobilization, permitting fixation and manipulation of living cell positions, while conventional physical and chemical cell immobilization can have adverse effects on cell functioning.

To extract the structural information of a trapped object, OT can be combined with spectroscopic techniques to measure the absorption, fluorescence and Raman spectra [21,142–145]. Raman spectroscopy analysis does not require labels to analyze and identify cells, thus presenting their viability. To obtain stable scattered light from a cell, Raman spectroscopy requires a relatively long time due to its low sensitivity. Combining this method with OT enables spatially fixing a cell over a long period time, bringing the advantage of obtaining the spectra from a single object instead of an ensemble of averages. The method excludes heterogeneity, providing information only about specific chemicals in the object [146]. OT with Raman spectroscopy can be combined with single- and dual-beam traps or an optical stretcher. An RBC consists of hemoglobin (Hb), a globular protein with an embedded porphyrin (heme group), which constitutes the Hb prosthetic component, with an iron atom for oxygen transfer. The chromophoric structure of the heme contributes to Raman scattering enhancement, with wavelengths close to the absorption bands [147]. The occurrence of resonance Raman scattering from the Hb prosthetic group allows studying Hb within erythrocytes without interference by other RBC components. Ramser et al. [148] combined Raman spectroscopy with OT in a microfluidic system to trap RBCs and monitor their oxygenation state in real time upon changes in the buffers with an electro-osmotic flow. The approach can be used for the cell response to any kind of treatment, for example, pharmaceutics, to monitor physical and chemical changes in cellular components.

Rao et al. [19] focused on the oxy/deoxy transition in a trapped RBC under mechanical stress (stretching and compression). UV–vis absorption spectroscopy supported the previous results, showing that single RBCs undergo a partial deoxygenation in the presence of local deformations induced by trapping beams. The mechanically induced chemical alterations, including Hb conformational changes, play the main role in the absorption state [149].

Polarized Raman spectroscopy provided evidence of an increased hemoglobin protein ordering upon RBC stretching with optical tweezers [150]. The polarization components of the scattered light were analyzed from the relaxed and stretched RBCs, confirming that during stretching, hemoglobin proteins are increasingly arranged in order Fig. 10(a, b). Further study by S. Ahlawat et al. [151] demonstrated the dependence of the Raman spectrum on the trapped RBC orientation. The Raman excitation beam is polarized along the x axis, and propagated along the z axis (Fig. 10(c)). The maximum heme bands were observed when the RBC's equatorial plane was parallel to the excitation beam polarization direction, while the minimum corresponded to the cell's plane being normal to the polarization direction. Authors therefore suggest, that Hb molecules must be present in an ordered arrangement, that heme-porphyrin planes become mostly orientated parallel to the equatorial plane.

The practical application of Raman tweezers was found in the quality control of blood reserves: the aging process of thrombocyte or erythrocyte concentrates was observed by Gangnus et al. [20]. The distinct change in platelets was confirmed between 8-day and 21-day concentrations in the wavenumber range of 1296–1333 cm^1. RBCs followed the same tendency; however, until day 21, no difference was observed. Cell decay started to occur in a donor-dependent way on day 28, day 32 and day 36. This Raman-trapping-based method analyzing blood samples in a quick and nondestructive manner shows promising application in the assessment of blood transfusion quality.

De Luca et al. [152] investigated thalassemic (a genetic defect in the hemoglobin structure) and normal RBCs with the use of

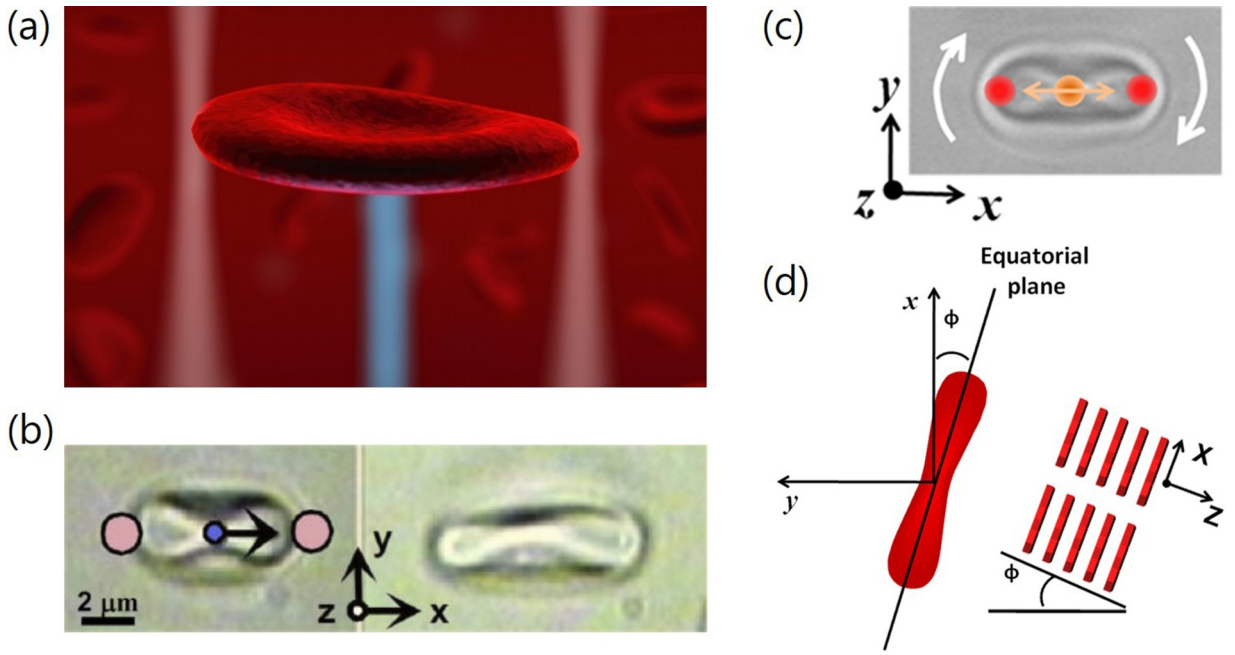

Fig. 10. (a) Two movable 1064-nm optical traps stretching an RBC while a 785-nm beam passes through its center, exciting the Raman scattering. (b) Two camera images show the cell in its equilibrium (left) and stretched (right) positions. All beams (circles) are directed into the (z)-axis, and the polarization direction (arrow) of the Raman excitation beam is in the plane of the cell, aligned with the direction of stretching (x). Image adapted from [150]. (c) An image of the trapped RBC captured by the camera, showing the direction of cell rotation, the red dots showing positions of the trapping beams, and the orange dot is the position of the Raman excitation beam. (d) Schematic showing the orientation angle ϕ which the equatorial plane of the trapped RBC made with the polarization direction of the Raman excitation beam, and hypothetical stacking of heme-porphyrin molecules with their planes parallel to the RBCs' equatorial plane. Reprinted from [151]. (For interpretation of the references to color in this figure legend, the reader is referred to the web version of this article.)

Raman OT to stretch them and cause stiffening. The thalassemic RBCs were 40% stiffer than the normal ones. The Raman spectra showed the reduced oxygenation capability of the Hb of thalassemic cells.

10. Cell sorting with OT

OT cell sorting is based on the creation of an optical intensity pattern over the sample area. Cells passing through this area can be sorted based on the intrinsic optical characteristics. Potential applications of an automated single-cell sorting system are the creation of cell patterns and biosensors, drug screening on a single-cell level, and a combination with molecular analysis. The single-cell sorter is assigned for the recovery of rare cells from aqueous suspensions. Compared to the existing methods, an OT-based cell sorter requires a reduced sample size, high positioning accuracy and contactless manipulation.

The first attempts at cell sorting with light were proposed by Imasaka et al. [10] with the method named "optical chromatography" [10]. A weakly focused laser beam was installed in a counterpropagating fluid flow. The scattering force from the laser beam pushed flowing particles into the focal point. This method was applied to separate blood cells by Kaneta et al. [11]. The single-cell sorting technique was developed and applied to sort out RBCs in a sample of human peripheral blood from other components (WBCs, platelets) based on size [12]. Erythrocytes were identified and manipulated into designated volumes using a counterpropagating dual-beam trap and an image-processing technique. Applegate et al. [13] performed the trapping of bovine RBCs by focusing a laser diode bar. The RBCs were directed at an angle to one of seven chosen flow streamlines. In the study by MacDonald et al. [14,153], RBCs were separated from lymphocytes based on their shape. The researchers used an angled optical lattice that can be extended to any general two- or three-dimensional potential energy landscape. Passive optical sorting (without fluid flow) was performed using the Bessel beam unique optical landscape [15]. At high powers, RBCs were locked into the outer rings of the Bessel beam (third, fourth and fifth), while spherically shaped lymphocytes rapidly moved directly toward the beam center and could be collected from the center core (Fig. 11).

11. Blood storage control with OT

Blood storage control is necessary for the safety of the samples used for medical treatment. OT enables identifying the changes in erythrocyte deformability properties during storage.

In a 2006 report [154], OT were proposed for the measurement of the apparent membrane viscosity, cell adhesion, zeta potential

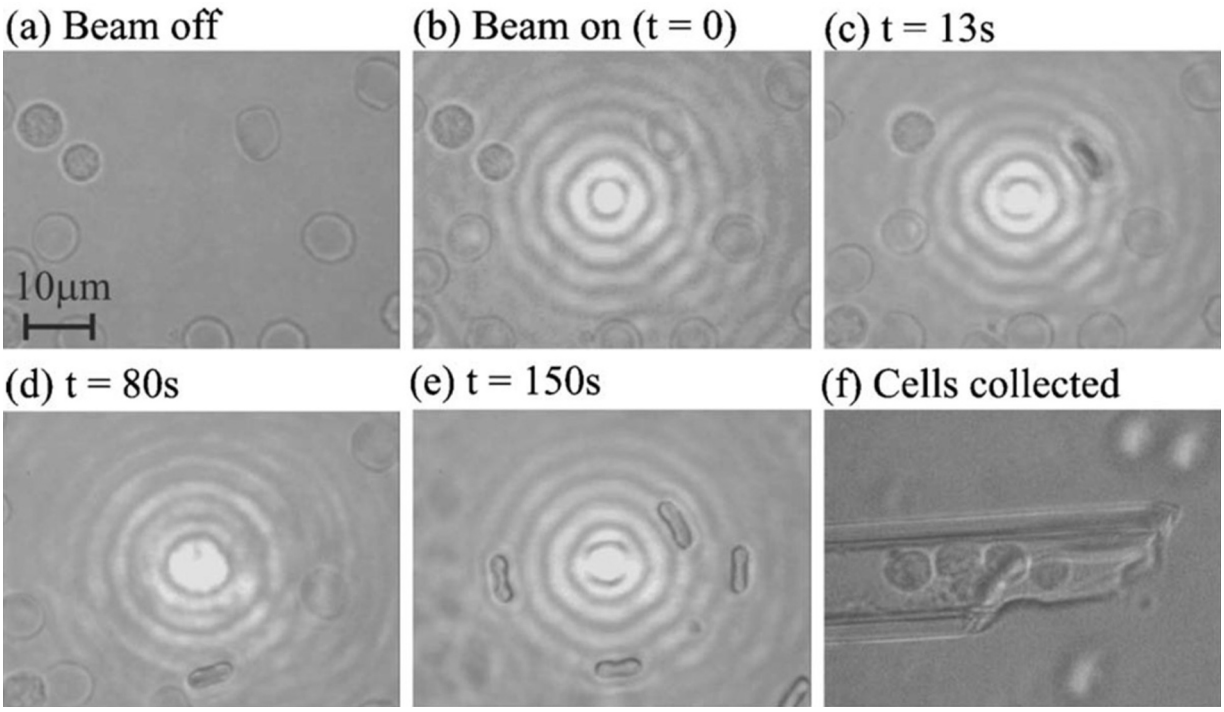

Fig. 11. A sample chamber containing an equal number of lymphocytes and RBCs [15]. (a) Two lymphocytes can be seen in the top-left corner, surrounded by erythrocytes. (b) The sample is exposed to a Bessel beam. (c) and (d) Cells are transported toward the central core. (e) The arrangement of cells at the top of the sample chamber with two lymphocytes aligned vertically in the beam center, and the RBCs, aligned with their largest axis in the direction of beam propagation, in the outer rings of the Bessel beam. (f) Lymphocytes can be extracted from the sample into a separate reservoir using a carefully positioned microcapillary.

and size of the double layer of charges. These RBC properties are important for the immunohematologic tests usually performed in blood banks. The control of blood properties during storage is necessary to ensure blood transfusion safety. When individuals with the sickle cell trait (HbAS) do not have any symptoms, they are eligible for blood donation. The blood from HbAS patients and those with sickle cell anemia (HbBS) was checked regarding the elasticity change during storage [155]. The results revealed higher elastic constants for HbAS and HnNS cells than those for healthy RBCs for up to 21 days of storage. However, HbAS became extremely rigid if stored for more than 28 days, suggesting preferable use of blood for transfusion before the 21st day of storage.

A method for measuring the RBC zeta potential was offered by [156]. By measuring the zeta potential, the RBC charge change during storage could be estimated. Elasticity measurements were performed by applying the drag force of blood plasma to a trapped RBC at different velocities. The cell length elongation under the flow force was registered with a camera and was then retrieved from the images. Based on the equilibrium equation, when an elastic force cancels the drag force, the apparent elasticity could be retrieved. RBC elasticity upon storage decreased slightly before day 22 ($4.1 \times 10^{-7} \pm 0.6 \times 10^{-7}$ N/m) and then dropped to the minimum value ($9.6 \times 10^{-7} \pm 1.0 \times 10^{-7}$ N/m), becoming 134% less deformable at the end of storage (day 36).

The same procedure was used by Barjas-Castro et al. [157] to estimate the influence of gamma irradiation on RBC biomechanical properties, since it is a common practice for the prophylaxis of transfusion-associated graft-versus-host disease (TA-GVHD). The analysis of RBC deformation demonstrated no difference with a control untreated sample up to 14 days. However, drastic rigidification occurred after 21 days (10-fold) and 28 days (40-fold). The alternative approach to the cell stretching method with two traps was implemented with one beam [158] by an acousto-optic modulator (AOM), which enabled focal point jumping along the normal to the beam axis to two fixed positions. The stable trapping and stretching of RBCs was performed for a jumping distance on the order of a few microns at frequencies exceeding 100 Hz.

A study conducted by Lukose et al. [159] demonstrated that the use of 0.9% normal saline for RBC storage caused oxygenation, in contrast to RBCs stored in a plasma solution.

12. OT applications for WBCs and platelets

12.1. T cells

OT are not suitable for measuring the passive mechanical properties of leukocytes due to cell activation, being deformed using their own chemical machinery. Studies of the active behavior of leukocytes, however, have been successfully performed. One of the first OT studies with leukocytes, we believe, was conducted in 1991 by Seeger et al. [26]. Lymphocyte T cells labeled anti-CD4

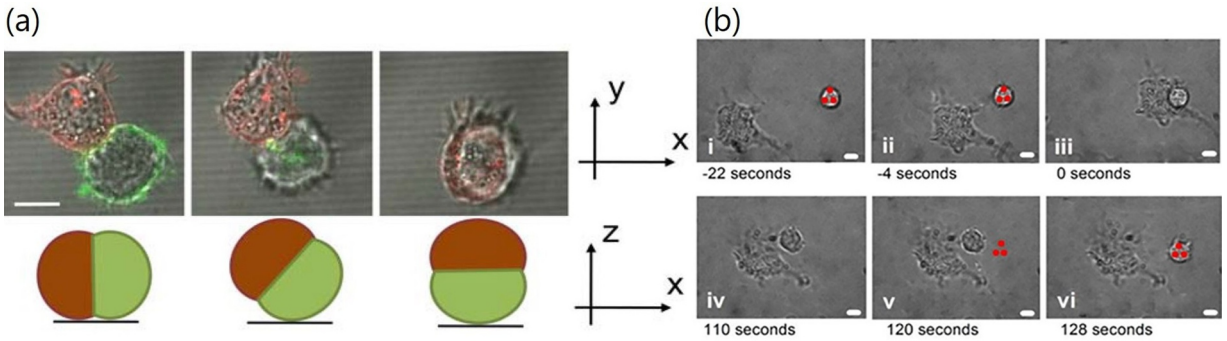

Fig. 12. (a) Fluorescence and transmitted light images of a natural killer (NK) cell (effector; green) and a T cell (target; red) synapse being manipulated into an imaging configuration such that the intercellular contact lies en face toward the imaging plane. Scale bar: 10 μm [160]. (b) The methodology used to study the interaction forces between T cells and dendritic cells. Red spots indicate the OT [161]. (For interpretation of the references to color in this figure legend, the reader is referred to the web version of this article.)

antibodies were first sorted into a microcapillary and then forced to make contact with a cancer erythroleukemia cell. The contact between the cells immediately (within 20 s) initiated morphological changes in the cancer cell, followed by oscillatory kinetics, which at present has only a speculative explanation, i.e., that this is an attempt of the erythroleukemia cell to repair the damage and counterattack the T cell.

Being conjugated with confocal microscopy, the OT allowed a high spatial resolution and high-speed imaging of the interface (immune synapse) between the natural killer (NK) cell (effector) and the T cell (target) [160] (Fig. 12(a)). This combination demonstrated the new extended opportunities compared to conventional sectioning.

A commonly applied approach is based on the stimulation of immune cells with antibody-coated beads. T cells were stimulated by probing them with antigen-presenting cells (APCs) - anti-CD3 mAb-coated beads - at different locations [162]. Observations showed that the leading edge of T cells appeared to be more sensitive than the tail. The lymphocyte response was also dependent on the antibody density on the bead.

A study by Anvari et al. [163] demonstrated how pseudopodia localization on lymphocytes is dependent on the application of mechanical stress with OT. Antibodies against T cell receptors (TCRs) bearing beads, upon the interaction with the lymphocyte TCR site, generated stress in a range of 100–250 pN. Simple attachment of the bead stimulates random pseudopodia formation, while a tangential force attracts pseudopodia to the site of stress.

Recently, another approach was introduced by Glass et al. [161], which does not require beads to measure the relative interaction forces between a dendritic cell and a T cell. A triple-spot optical trap ensured the fixed positioning of the T cell, excluding rolling and rotation. The trapped cell was brought into contact with a dendritic cell (Fig. 12(b)) to break the linkage between the cells, which can be time-dependent. The trap was placed in the vicinity of the cell, and the power was increased slowly, until the T cell again fell into the trap. This method can be applied to different types of cells to reveal the effects of the contact time, drug treatment, etc.

Mannie at al. [164] applied OT to fix T cells to register the Raman spectra of an individual cell to reveal the activation status. The same beam at 785 nm was used to trap and excite the cell, with the obtained spectra allowing the activated cells to be distinguished from the other cells.

A deep analysis of the TCR mechanosensing findings obtained via optical trapping can be found in the extensive review by Feng et al. [165].

Another technical solution - a combination of total internal reflection fluorescence (TIRFM) and optical trapping - was presented by Snijder-Van at al. [166]. In that configuration, a cell can be placed on the surface under the objective, allowing for spatial control of the interactions between the cell and site of interest with OT while monitoring the process with the TIRFM.

12.2. Neutrophils

OT were used to mimic the shear forces experienced by neutrophils in vivo. A laser beam (980-nm wavelength) dragged through a polymorphonuclear leukocyte membrane triggered an influx of extracellular calcium in the cell, suggesting a link between mechanical stress and calcium influx [167].

While most methods focus on trapping whole cells, an alternative approach was offered by Yanai et al. [25]. Using an OT system coupled with a differential interference contrast microscope, they were able to trap intracellular granules inside neutrophils. Trapped granules were moved in viscoelastic cytoplasm in different regions of a neutrophil. The elastic modulus and viscosity were then retrieved from the dynamic force and granule displacement measurements. The same group later proceeded to distinguish the rheological differences inside a cell, concluding that leading edge of the neutrophil is more fluid-like and less stiff than the body and trailing regions [168].

The adhesion of leukocytes to the vascular endothelium was studied by measuring the force-distance relationship of THP-1 cells and HUVEC monolayer detachment [169]. The force spectroscopy trace (force dependence on distance) demonstrated the stretch-rupture events and revealed the effect of yielding, which is characteristic of nonelastic materials.

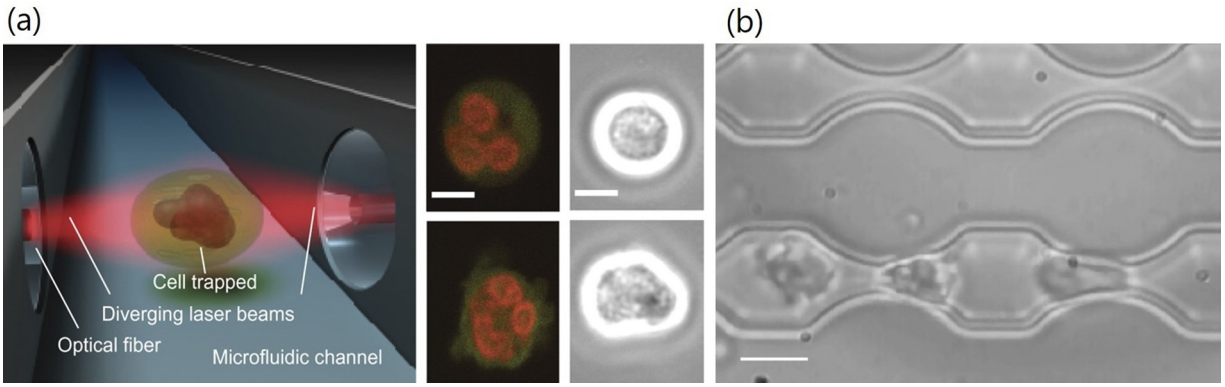

Fig. 13. (a) OS with two counterpropagating laser beams emanating from single-mode optical fibers: confocal images and phase contrast images of the trapped neutrophils. The resting cells remain round (top), whereas the activated cells have amoeboid shapes (bottom). Scale bar: 5 μm. (b) Microcirculation mimesis with neutrophils flowing through the channels. Scale bar: 10 μm. Reproduced from [170].

Neutrophils passing through microcapillaries of the pulmonary system continuously experience shear stress and stretching; however, not all of them are activated. Upon activation, neutrophils become polarized and of amoeboid shape. By multiple oscillatory deformation of neutrophils in an OS, and with confocal and phase contrast image analysis ((Fig. 13(a)), Ekpenyong et al. [170] observed the starting stage of activation. Interestingly, under continuous stress, the process turned out to be reversible. Neutrophils demonstrated the same behavior in special microcirculation mimesis with physical borders of the microfluidic chamber as that under OS-generated stress (Fig. 13(b)).

13. Other applications of OT in blood studies

Overcoming the photodamage problem [91], Liang et al. [171] developed OT based on “tug-of-war” (TOW) beams. Diverging and elongated beams created with a spatial light modulator provided more efficient trapping with less photodamage than a conventional dual-OT system. This geometry allowed RBC stretching and squeezing. Using this method, the researchers found that RBC deformability under different osmotic conditions follows the following trend: hypotonic > isotonic > hypertonic (Fig. 14).

The birefringent nature of RBCs was suggested because of the orientation they take in an optical trap. An RBC acquires an edge-on orientation in the beam propagation direction. In the case of linearly polarized OT, an RBC stays rotationally bound to the direction of polarization. The birefringence of RBCs was found to be confined in the dimple region, with the slow axis of RBCs being along the diameter [172]. According to the observations made with a polarizing microscope, the expected retardation revealed by the

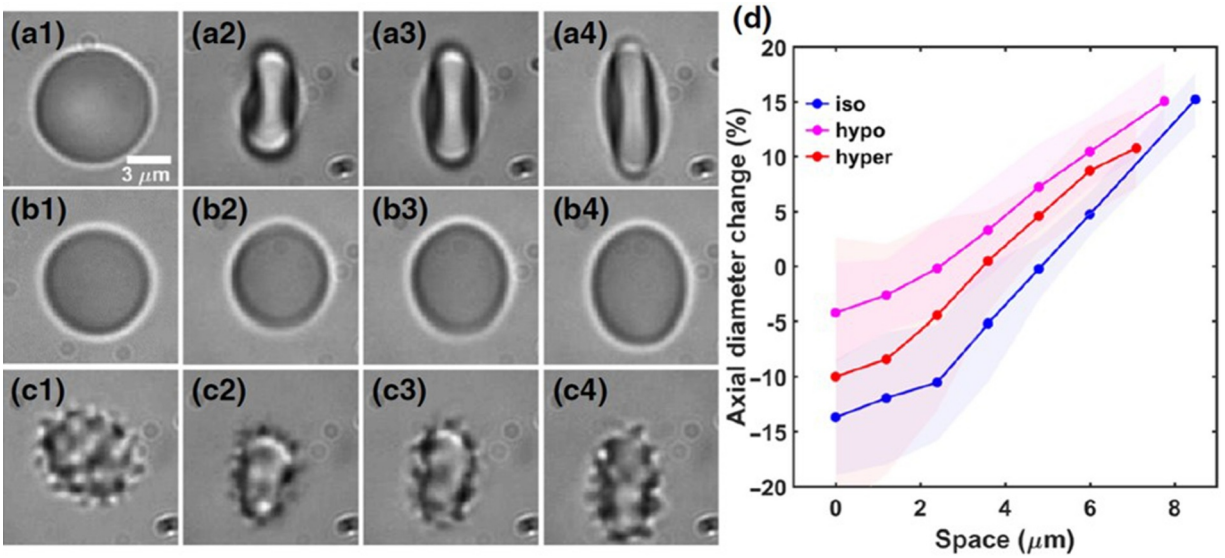

Fig. 14. RBC stretching in different buffers: (a1–a4) isotonic, (b1–b4)) hypotonic, and (c1–c4) hypertonic. The spacing between two arms of the “tug-of-war” (TOW) tweezers is varied, while the laser power at the focal plane is fixed at 40 mW. The first column: images without trapping. Columns from the second to the fourth illustrate the RBC shape change when the spacing is 2.4, 4.8 μm and the maximum 8 (c4) - 9.8 (a4) μm, respectively. (d) Percentage change of the axial diameter of RBCs as a function of the spacing between two arms of the TOW beam [171].

optomechanical response of the RBCs in the OT was 1.87 ± 0.09 nm. This was confirmed by the time estimation needed for RBC alignment when the polarization plane is rotated with a half-wave plate. The origin of RBC birefringence was related to the phospholipid content of the lipid bilayer in the RBC membrane because RBCs suspected to exhibit crenation demonstrated diminishing birefringence, along with deceleration of the response in OT.

Jumping OT were used to measure RBC deformability after an arterial occlusion test (AOT) to characterize tissue oxygenation [173]. According to the observations, more oxygenated RBCs were more deformable, being able to deliver more oxygen to muscle tissue when passing through narrow microvessels. The change in hemoglobin concentration dominates the correlation between the erythrocyte elastic constant and the dynamic tissue oxygenation induced by the AOT. The acquired data highlights the importance of correlating the contribution of the RBC elastic properties with the supply of oxygen to tissues.

Drug-induced softening of the RBC membrane was detected with OT after atorvastatin (a commonly prescribed statin drug) treatment [174], suggesting direct interactions between the drug and cytoskeletal components. OT used in biology utilize a continuous wave (CW); however, femtosecond OT have also been developed, which can be used without damaging the RBCs [175]. Compared to the CW laser, no differences were observed in the trapping efficiency of OT. Zhou et al. used a 800-nm femtosecond Ti:sapphire laser to stably trap RBCs and showed the ability to make them rotate inside the trap by modulating the laser light intensity [176]. The nonequilibrium nature of RBC flickering was demonstrated [177] by trapping RBCs with four beads. One of the beads allows detecting free fluctuations or the mechanical response to the applied force measurement, while the other three keep the RBC in a stable position.

14. In vivo RBC trapping

Biomechanics was found to have essential interplay with cell functioning; hence, OT became one of the most convenient tools for living cell studies. In addition to a wide panel of OT applications in vitro, where the conditions for accurate measurements can be controlled, the need for in vivo measurements is growing to enable dynamic force measurements in realistic conditions [178].

The first in vivo RBC manipulation was presented by Zhong et al. [179]. NIR OT were able to trap RBCs in a ~ 5–16 μm blood capillary beneath ~ 40 μm in a mouse ear. The power used to trap the cell was 168 mW. By trapping and holding an RBC, an artificial clot was induced, which was removed again with OT to restore normal flow. The optical trap stiffness in vivo was ~ 10 pN/μ^{-1}. Trapping was limited to a depth of ~ 40 μm, since optical stiffness largely varies at different locations due to the complex composition of biological tissue.

Subsequent studies sought to circumvent the difficulties in obtaining quantitative values and calibration for in vivo optical manipulation using zebrafish embryos. Zebrafish, being optically transparent, became a widely used model for studying the processes of disease development in nanomedicine fields. Pioneering results were provided by the quantitative optical trapping of data in vivo using the combination of OT with fast imaging and a numerical simulation [180]. The study demonstrated the importance of microvasculature viscoelasticity in zebrafish arterial blood flow. Analyzing the behavior of trapped RBCs at different positions in the vasculature, the authors obtained an optical force map of the flow. The displacements of the trapped RBCs were found to correlate with endothelial cell wall movement, suggesting that vasculature viscoelasticity mediates the flow. Another study of the same group based on the same approach [181] showed the adhesion of epicardial cells to the pericardium during cardiac development. It revealed that hydrodynamic flow forces control organogenesis. The group then presented a methodology for the accurate calibration of trap stiffness in vivo [182]. Measurements of the flow profiles and drag forces exerted on the tweezed cell in the vasculature allowed characterization of the hemodynamic forces.

In vivo cell transportation is of high interest for precision medicine and drug delivery. To circumvent the influence of a complex environment restricting the transportation process in vivo, Liu et al. [183] developed an automated control to avoid collisions and obstacles. The approach was demonstrated by moving RBCs in zebrafish. However, it can be applied to different environments.

In the study of Johansen et al., trapped RBCs were brought in contact with vasculature walls to estimate adhering forces. Injected NPs (100, 200, 500 and 1000 nm) adhered to the capillary walls, causing deformation. To trap the NPs, the laser power at the sample was 75 mW, while a power of 250 mW was used for the RBCs at a depth of approximately 50 μm (Fig. 15). The offered method gives insights into the cell interactions in vivo and the potential for NP-cell interaction screening in nanomedicine.

Development toward in vivo OT applications is underway. A step forward was achieved with the development of single-beam acoustic tweezers (SBAT), which can penetrate deeply into biological tissues without causing damage using a 50-MHz ultrasound transducer driven by a voltage signal generator [184]. Test experiments demonstrated that RBCs can be trapped in mimicking in vivo conditions a 2-μm diameter microvessel with flowing RBCs suspended in blood plasma. The SBAT managed to trap RBCs at a flow speed of 7.9 cm/s, which is higher than that in capillaries (0.03 cm/s) and close to the mean blood flow in arterioles and venules (5 to 10 cm/s) [185]. OT were also applied to identify the cell type and measure the adhesion of cells to an autologous graft intended for the replacement of diseased blood vessels and for bypass surgery [186].

15. Summary

The utilization of OT is a continuously evolving technique that has proved its importance in a wide range of studies and never ceases to offer new research opportunities. Not only the technical improvements of OT themselves but also their combination with other methods have resulted in profound contributions to blood cell science. OT have thus far mainly been applied in fundamental research; however, the method has the potential to be transferred to applied medicine. Still, there are limitations that should be addressed to expand OT applicability:

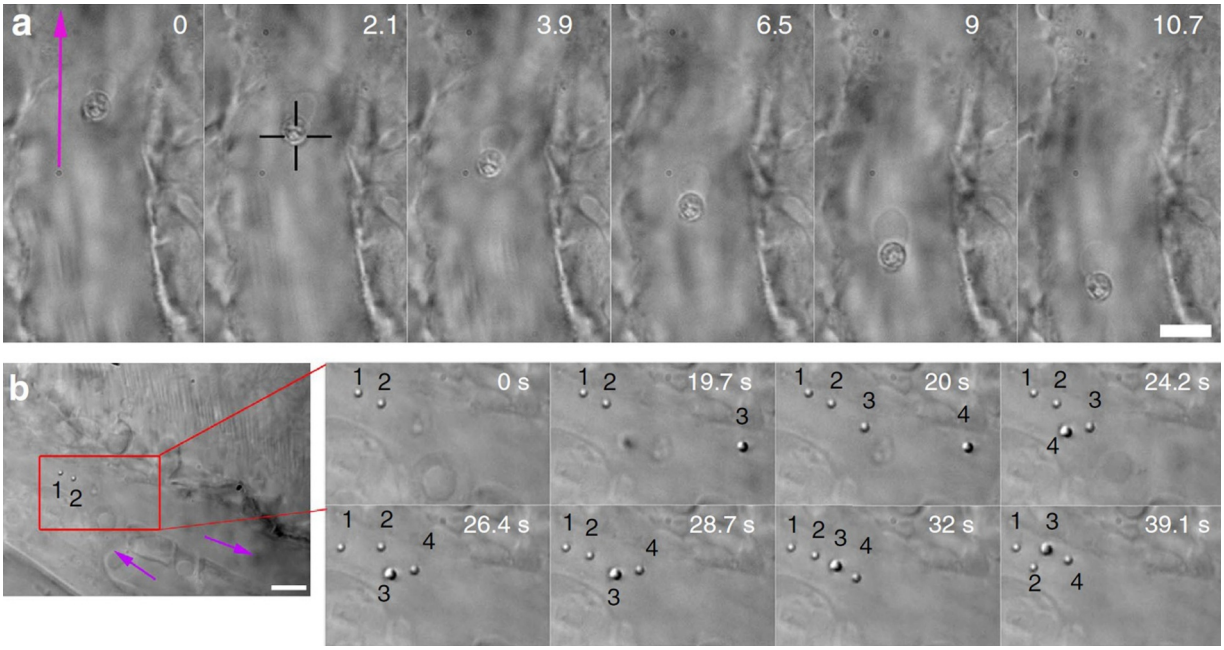

Fig. 15. *In vivo* optical micromanipulation of microinjected particles [187]. Separate particles (numbered) are fished out of the blood flow and moved toward a sheltered region at the tip of the tail. The purple arrows indicate the flow direction. Scale bar: 5 μm. (For interpretation of the references to color in this figure legend, the reader is referred to the web version of this article.)

1. **Limited depth for in vivo measurements**. Living tissue scatters and absorbs light; therefore, the maximum depth of trapping in vivo achieved thus far is 50 μm [187].
2. **Statistically trustworthy results**. Combination of OT with microfluidics and the previously mentioned optical stretcher method can significantly reduce the time of data acquisition [24].
3. **Trained manipulator and standardization**. The manipulation complexity depends on the type of experiment. Currently, versatile commercial OT do not require special operation skills, as do most advanced solutions by Lumicks. Indeed, the measurement protocols differ from one study to another, emphasizing the need to develop uniform approaches. A calibration approach applicable to living systems has also been introduced [182].
4. **Limited force range**. OT are known to work in a pN range, but the force load can be increased up to nN by using anti-reflection-coated microspheres [188].
5. **Portability**. Technical solutions, such as compact lasers, fiber lasers, and a new design, can result in portable OT.

OT combined with other modalities should hasten the adoption of lab-on-chip devices for diagnostics, sensing, testing and drug discovery. To contribute to future blood microcirculation monitoring and therapy, OT assisted methods can be used as a first-pass diagnostic test.

Declaration of Competing Interest

None.

CRediT authorship contribution statement

Tatiana Avsievich: Writing - review & editing, Writing - original draft, Conceptualization, Writing - original draft, Writing - review & editing. **Ruixue Zhu:** Writing - review & editing. **Alexey Popov:** Writing - review & editing. **Alexander Bykov:** Writing - review & editing. **Igor Meglinski:** Conceptualization, Writing - review & editing.

Acknowledgments

Tatiana Avsievich acknowledges Suomen Kulttuurirahasto (Grant no. 00190188, 2021). Ruixue Zhu acknowledges the China Scholarship Council (CSC no. 201706410089, R.Z.) and Tauno Tnning Foundation (Grant no. 20190104, R.Z.). Alexey Popov acknowledges partial support from the Academy of Finland (projects 32126, 334531). Professor Meglinski acknowledges partial support from the INFOTECH, Academy of Finland (project 325097), the MEPhI Academic Excellence Project (Contract no.

02.a03.21.0005) and the National Research Tomsk State University Academic D.I. Mendeleev Fund Program. The authors also acknowledge the contribution of the Russian Science Foundation (Project: 19-72-30012).

References

[1] A. Ashkin, Acceleration and trapping of particles by radiation pressure, Phys. Rev. Lett. 24 (4) (1970) 156.
[2] J. Kepler, De Cometis Libelli Tres, Typis Andreae Apergeri, Sumptibus Sebastiani Mylii Bibliopolae Augustani, Avgvstae Vindelicorum, 1619.
[3] P. Lebedew, Untersuchungen über die druckkräfte des lichtes, Ann. Phys. 311 (11) (1901) 433–458.
[4] A. Ashkin, J. Dziedzic, J.E. Bjorkholm, S. Chu, Observation of a single-beam gradient force optical trap for dielectric particles, Opt. Lett. 11 (5) (1986) 288–290.
[5] A. Ashkin, J.M. Dziedzic, T. Yamane, Optical trapping and manipulation of single cells using infrared laser beams, Nature 330 (6150) (1987) 769.
[6] N.M.A. 2019, Arthur Ashkin facts, 2019, (https://www.nobelprize.org/prizes/physics/2018/ashkin/facts/).
[7] H. Zhang, K.-K. Liu, Optical tweezers for single cells, J. R. Soc. Interface 5 (24) (2008) 671–690.
[8] K.O. Greulich, Manipulation of cells with laser microbeam scissors and optical tweezers: a review. Rep. Prog. Phys. 80 (2) (2017) 026601.
[9] G. Bao, S. Suresh, Cell and molecular mechanics of biological materials, Nat. Mater. 2 (11) (2003) 715–725.
[10] T. Imasaka, Y. Kawabata, T. Kaneta, Y. Ishidzu, Optical chromatography, Anal. Chem. 67 (11) (1995) 1763–1765.
[11] T. Kaneta, Y. Ishidzu, N. Mishima, T. Imasaka, Theory of optical chromatography, Anal. Chem. 69 (14) (1997) 2701–2710.
[12] S.C. Grover, A.G. Skirtach, R.C. Gauthier, C.P. Grover, Automated single-cell sorting system based on optical trapping, J. Biomed. Opt. 6 (1) (2001) 14–23.
[13] R.W. Applegate, J. Squier, T. Vestad, J. Oakey, D.W. Marr, Optical trapping, manipulation, and sorting of cells and colloids in microfluidic systems with diode laser bars, Opt. Express 12 (19) (2004) 4390–4398.
[14] M.P. MacDonald, G.C. Spalding, K. Dholakia, Microfluidic sorting in an optical lattice, Nature 426 (6965) (2003) 421.
[15] L. Paterson, E. Papagiakoumou, G. Milne, V. Garcés-Chávez, S. Tatarkova, W. Sibbett, F.J. Gunn-Moore, P. Bryant, A.C. Riches, K. Dholakia, Light-induced cell separation in a tailored optical landscape, Appl. Phys. Lett. 87 (12) (2005) 123901.
[16] T. Yang, F. Bragheri, P. Minzioni, A comprehensive review of optical stretcher for cell mechanical characterization at single-cell level, Micromachines 7 (5) (2016) 90.
[17] S. Sato, M. Ishigure, H. Inaba, Optical trapping and rotational manipulation of microscopic particles and biological cells using higher-order mode Nd: Yag laser beams, Electron. Lett. 27 (20) (1991) 1831–1832.
[18] S. Henon, G. Lenormand, A. Richert, F. Gallet, A new determination of the shear modulus of the human erythrocyte membrane using optical tweezers, Biophys. J. 76 (2) (1999) 1145–1151.
[19] S. Rao, Š. Bálint, B. Cossins, V. Guallar, D. Petrov, Raman study of mechanically induced oxygenation state transition of red blood cells using optical tweezers, Biophys. J. 96 (1) (2009) 209–216.
[20] R. Gangnus, K. Schütze, J. Luhm, M. Johnsen, T. Tonn, Raman-spektroskopie zur qualitätskontrolle von blutprodukten, BioPhot. 1 (1) (2014) 22–25.
[21] Y. Liu, G. Sonek, M. Berns, K. Konig, B. Tromberg, Two-photon fluorescence excitation in continuous-wave infrared optical tweezers, Opt. Lett. 20 (21) (1995) 2246–2248.
[22] I. Sraj, C.D. Eggleton, R. Jimenez, E.E. Hoover, J.A. Squier, J. Chichester, D.W. Marr, Cell deformation cytometry using diode-bar optical stretchers, J. Biomed. Opt. 15 (4) (2010) 047010.
[23] I. Sraj, D.W. Marr, C.D. Eggleton, Linear diode laser bar optical stretchers for cell deformation, Biomed. Opt. Express 1 (2) (2010) 482–488.
[24] Z. Yao, C.C. Kwan, A.W.O.W. Poon, An optofluidic ǣtweeze-and-dragg cell stretcher in a microfluidic channel, Lab Chip (2020).
[25] M. Yanai, J.P. Butler, T. Suzuki, A. Kanda, M. Kurachi, H. Tashiro, H. Sasaki, Intracellular elasticity and viscosity in the body, leading, and trailing regions of locomoting neutrophils, Am. J. Physiol. Cell Physiol. 277 (3) (1999) C432–C440.
[26] S. Seeger, S. Monajembashi, K.-J. Hutter, G. Futterman, J. Wolfrum, K. Greulich, Application of laser optical tweezers in immunology and molecular genetics, Cytometry 12 (6) (1991) 497–504.
[27] A. Ashkin, Forces of a single-beam gradient laser trap on a dielectric sphere in the ray optics regime, Biophys. J. 61 (2) (1992) 569–582.
[28] K. Dholakia, P. Reece, M. Gu, Optical micromanipulation, Chem. Soc. Rev. 37 (1) (2008) 42–55.
[29] M.J. Lang, S.M. Block, Resource letter: Lbot-1: Laser-based optical tweezers, Am. J. Phys. 71 (3) (2003) 201–215.
[30] I. Verdeny, A. Farré, J. Mas Soler, C. López Quesada, E. Martín Badosa, M. Montes Usategui, Optical trapping: a review of essential concepts, Ópt. Pura Aplicada 44 (3) (2011) 527–551.
[31] S. Wei, W. Yi-Qiu, G. Chong-Ming, Construction of an optical tweezerscalculation and experiments, Chin. Phys. 9 (11) (2000) 855.
[32] D.G. Grier, A revolution in optical manipulation, Nature 424 (6950) (2003) 810.
[33] M.D. Koch, J.W. Shaevitz, Introduction to optical tweezers, Optical Tweezers, Springer, 2017, pp. 3–24.
[34] J.E. Molloy, M.J. Padgett, Lights, action: optical tweezers, Contemp. Phys. 43 (4) (2002) 241–258.
[35] P. Polimeno, A. Magazzu, M.A. Iatì, F. Patti, R. Saija, C.D.E. Boschi, M.G. Donato, P.G. Gucciardi, P.H. Jones, G. Volpe, et al., Optical tweezers and their applications, J. Quant. Spectrosc. Radiat. Transf. 218 (2018) 131–150.
[36] A. Ashkin, J. Dziedzic, Optical trapping and manipulation of single living cells using infra-red laser beams, Berichte Bunsengesellschaft Physikalische Chemie 93 (3) (1989) 254–260.
[37] Y. Harada, T. Asakura, Radiation forces on a dielectric sphere in the rayleigh scattering regime, Opt. Commun. 124 (5–6) (1996) 529–541.
[38] G. Gouesbet, J. Lock, G. Gréhan, Generalized Lorenz–Mie theories and description of electromagnetic arbitrary shaped beams: localized approximations and localized beam models, a review, J. Quant. Spectrosc. Radiat. Transf. 112 (1) (2011) 1–27.
[39] J.A. Lock, Calculation of the radiation trapping force for laser tweezers by use of generalized Lorenz-Mie theory. I. Localized model description of an on-axis tightly focused laser beam with spherical aberration, Appl. Opt. 43 (12) (2004) 2532–2544.
[40] F. Borghese, P. Denti, R. Saija, M.A. Iati, Optical trapping of nonspherical particles in the T-matrix formalism, Opt. Express 15 (19) (2007) 11984–11998.
[41] A. Ashkin, Optical Trapping and Manipulation of Neutral Particles Using Lasers: A Reprint Volume with Commentaries, World Scientific, 2006.
[42] J. van Mameren, G.J.L. Wuite, I. Heller, Introduction to optical tweezers: background, system designs, and commercial solutions, Single Molecule Analysis, Springer, 2011, pp. 1–20.
[43] G. Volpe, L. Kurz, A. Callegari, G. Volpe, S. Gigan, Speckle optical tweezers: micromanipulation with random light fields, Opt. Express 22 (15) (2014) 18159–18167.
[44] C. Xie, M.A. Dinno, Y. Li, Near-infrared Raman spectroscopy of single optically trapped biological cells, Opt. Lett. 27 (4) (2002) 249–251.
[45] A.I. Bishop, T.A. Nieminen, N.R. Heckenberg, H. Rubinsztein-Dunlop, Optical microrheology using rotating laser-trapped particles, Phys. Rev. Lett. 92 (19) (2004) 198104.
[46] M.G. Donato, J. Hernandez, A. Mazzulla, C. Provenzano, R. Saija, R. Sayed, S. Vasi, A. Magazzù, P. Pagliusi, R. Bartolino, et al., Polarization-dependent optomechanics mediated by chiral microresonators, Nat. Commun. 5 (2014) 3656.
[47] M. Padgett, R. Bowman, Tweezers with a twist, Nat. Photon 5 (6) (2011) 343.
[48] D.C. Appleyard, K.Y. Vandermeulen, H. Lee, M.J. Lang, Optical trapping for undergraduates, Am. J. Phys. 75 (1) (2007) 5–14.
[49] C.J. Firby, K.N. Smith, S.R. Gilroy, A. Porisky, A.Y. Elezzabi, Design of a simple, low-cost, computer-controlled, dual-beam optical tweezer system, Optik 127 (1) (2016) 440–446.
[50] G. Pesce, G. Volpe, O.M. Maragó, P.H. Jones, S. Gigan, A. Sasso, G. Volpe, Step-by-step guide to the realization of advanced optical tweezers, JOSA B 32 (5) (2015) B84–B98.
[51] W.M. Lee, P.J. Reece, R.F. Marchington, N.K. Metzger, K. Dholakia, Construction and calibration of an optical trap on a fluorescence optical microscope, Nat. Protoc. 2 (12) (2007) 3226.

[52] M. Mathew, S. Santos, D. Zalvidea, P. Loza-Alvarez, Multimodal optical workstation for simultaneous linear, nonlinear microscopy and nanomanipulation: upgrading a commercial confocal inverted microscope, Rev. Sci. Instrum. 80 (7) (2009) 073701.
[53] R. Kosinski, A. Mukhortava, W. Pfeifer, A. Candelli, P. Rauch, B. Saccà, Sites of high local frustration in DNA origami, Nat. Commun. 10 (1) (2019) 1–12.
[54] M.A. Taylor, M. Waleed, A.B. Stilgoe, H. Rubinsztein-Dunlop, W.P. Bowen, Enhanced optical trapping via structured scattering, Nat. Photon. 9 (10) (2015) 669.
[55] K.C. Neuman, S.M. Block, Optical trapping, Rev. Sci. Instrum. 75 (9) (2004) 2787–2809.
[56] R.W. Bowman, M.J. Padgett, Optical trapping and binding, Rep. Prog. Phys. 76 (2) (2013) 026401.
[57] E.J. Corwin, Corwin, Handbook of Pathophysiology, Wolters Kluwer Health/Lippincott Williams & Wilkins, 2008.
[58] C.-H. Ho, White blood cell and platelet counts could affect whole blood viscosity, J. Chin. Med. Assoc. 67 (8) (2004) 394–397.
[59] H.F. Langer, T. Chavakis, Leukocyte–endothelial interactions in inflammation, J. Cell. Mol. Med. 13 (7) (2009) 1211–1220.
[60] N. Kang, Q. Guo, E. Islamzada, H. Ma, M.D. Scott, Microfluidic determination of lymphocyte vascular deformability: effects of intracellular complexity and early immune activation, Integr. Biol. 10 (4) (2018) 207–217.
[61] J. Sheriff, D. Bluestein, G. Girdhar, J. Jesty, High-shear stress sensitizes platelets to subsequent low-shear conditions, Ann. Biomed..Eng 38 (4) (2010) 1442–1450.
[62] R. Zhu, T. Avsievich, A. Popov, I. Meglinski, Optical tweezers in studies of red blood cells, Cells 9 (3) (2020) 545.
[63] N. Mohandas, P.G. Gallagher, Red cell membrane: past, present, and future, Blood 112 (10) (2008) 3939–3948.
[64] N. Mohandas, M.R. Clark, M.S. Jacobs, S.B. Shohet, Analysis of factors regulating erythrocyte deformability, J. Clin. Invest. 66 (3) (1980) 563–573.
[65] I. Safeukui, P.A. Buffet, G. Deplaine, S. Perrot, V. Brousse, A. Ndour, M. Nguyen, O. Mercereau-Puijalon, P.H. David, G. Milon, et al., Quantitative assessment of sensing and sequestration of spherocytic erythrocytes by the human spleen, Blood 120 (2) (2012) 424–430.
[66] M. Diez-Silva, M. Dao, J. Han, C. Lim, S. Suresh, Shape and biomechanical characteristics of human red blood cells in health and disease, MRS Bull. 35 (5) (2010) 382–388.
[67] E. Moeendarbary, A.R. Harris, Cell mechanics: principles, practices, and prospects, WIREs Syst. Biol. Med. 6 (5) (2014) 371–388.
[68] J. Kim, H. Lee, S. Shin, Advances in the measurement of red blood cell deformability: a brief review, J. Cell. Biotechnol. 1 (1) (2015) 63–79.
[69] G. Lenormand, S. Hénon, A. Richert, J. Siméon, F. Gallet, Direct measurement of the area expansion and shear moduli of the human red blood cell membrane skeleton, Biophys. J. 81 (1) (2001) 43–56.
[70] R.M. Hochmuth, R.E. Waugh, Erythrocyte membrane elasticity and viscosity, Annu. Rev. Physiol. 49 (1) (1987) 209–219.
[71] E.A. Evans, Bending elastic modulus of red blood cell membrane derived from buckling instability in micropipet aspiration tests, Biophys. J. 43 (1) (1983) 27–30.
[72] E.A. Evans, R. Waugh, L. Melnik, Elastic area compressibility modulus of red cell membrane, Biophys. J. 16 (6) (1976) 585–595.
[73] O.K. Baskurt, H.J. Meiselman, Blood rheology and hemodynamics, Seminars in Thrombosis and Hemostasis, 29 (2003), pp. 435–450.
[74] O.K. Baskurt, M.R. Hardeman, M.W. Rampling, Handbook of Hemorheology and Hemodynamics, volume 69, 2007. Ios Pr Inc; 1 edition.
[75] K. Tsukada, C. Sekizuka E.and Oshio, H. Minamitani, Direct measurement of erythrocyte deformability in diabetes mellitus with a transparent microchannel capillary model and high-speed video camera system, Microvasc. Res. 61 (3) (2001) 231–239.
[76] M. Wiewiora, K. Sosada, M. Wylezol, L. Slowinska, W. Zurawinski, Red blood cell aggregation and deformability among patients qualified for bariatric surgery, Obes. Surg. 17 (3) (2007) 365–371.
[77] S.M. Hosseini, J.J. Feng, How malaria parasites reduce the deformability of infected red blood cells, Biophys. J. 103 (1) (2012) 1–10.
[78] G.A. Barabino, M.O. Platt, D.K. Kaul, Sickle cell biomechanics, Annu. Rev. Biomed. 12 (2010) 345–367.
[79] M. Fornal, R.A. Korbut, M. Lekka, G. Pyka-Fościak, B. Wizner, J. Styczen, T. Grodzicki, Rheological properties of erythrocytes in patients with high risk of cardiovascular disease, Clin. Hemorheol. Microcirc. 39 (1–4) (2008) 213–219.
[80] W. Meier, M. Paulitschke, D. Lerche, G. Schmidt, K. Zoellner, Action of rHuEpo on mechanical membrane properties of red blood cells in children with end-stage renal disease, Nephrol. Dial. Transpl. 6 (2) (1991) 110–116.
[81] S. Lee, N. Kim, K. Sun, J. Dobbe, M. Hardeman, J. Antaki, K. Ahn, S. Lee, Association between arterial stiffness and the deformability of red blood cells (RBCs), Clin. Hemorheol. Micro. 34 (4) (2006) 475–481.
[82] L. Da Costa, J. Galimand, O. Fenneteau, N. Mohandas, Hereditary spherocytosis, elliptocytosis, and other red cell membrane disorders, Blood Rev. 27 (4) (2013) 167–178.
[83] O. Baskurt, B. Neu, H.J. Meiselman, Red Blood Cell Aggregation, CRC Press, 2011.
[84] E.H. Eylar, M.A. Madoff, O. Brody, J. Oncley, The contribution of sialic acid to the surface charge of the erythrocyte, J. Biol. Chem. 237 (6) (1962) 1992–2000.
[85] H.P. Fernandes, C.L. Cesar, M.d.L. Barjas-Castro, Electrical properties of the red blood cell membrane and immunohematological investigation, Rev. Bras. Hematol. Hemoter. 33 (4) (2011) 297–301.
[86] P. Bronkhorst, G. Streekstra, J. Grimbergen, E. Nijhof, J. Sixma, G. Brakenhoff, A new method to study shape recovery of red blood cells using multiple optical trapping, Biophys. J. 69 (5) (1995) 1666–1673.
[87] G. Késmárky, P. Kenyeres, M. Rábai, K. Tóth, Plasma viscosity: a forgotten variable, Clin. Hemorheol. Micro. 39 (1–4) (2008) 243–246.
[88] J.-J. Foo, V. Chan, Z.-Q. Feng, K.-K. Liu, Human red blood cells deformed under thermal fluid flow, Biomed. Mater. 1 (1) (2006) 1.
[89] R. Waugh, E. Evans, Thermoelasticity of red blood cell membrane, Biophys. J. 26 (1) (1979) 115–131.
[90] L. Miccio, P. Memmolo, F. Merola, P. Netti, P. Ferraro, Red blood cell as an adaptive optofluidic microlens, Nat. Commun. 6 (2015) 6502.
[91] M.A. de Oliveira, D.S. Moura, A. Fontes, R.E. de Araujo, Damage induced in red blood cells by infrared optical trapping: an evaluation based on elasticity measurements, J. Biomed. Opt. 21 (7) (2016) 75012.
[92] S. Grover, R.C. Gauthier, A. Skirtach, Analysis of the behaviour of erythrocytes in an optical trapping system, Opt. Express 7 (13) (2000) 533–539.
[93] K.S. Mohanty, S.K. Mohanty, S. Monajembashi, K.O. Greulich, Orientation of erythrocytes in optical trap revealed by confocal fluorescence microscopy, Biomed. Opt. 12 (6) (2007) 060506.
[94] A. Ghosh, S. Sinha, J. Dharmadhikari, S. Roy, A. Dharmadhikari, J. Samuel, S. Sharma, D. Mathur, Euler buckling-induced folding and rotation of red blood cells in an optical trap, Physical. Biol. 3 (1) (2006) 67.
[95] K. Svoboda, C.F. Schmidt, D. Branton, S.M. Block, Conformation and elasticity of the isolated red blood cell membrane skeleton, Biophys. J. 63 (3) (1992) 784–793.
[96] J. Sleep, D. Wilson, R. Simmons, W. Gratzer, Elasticity of the red cell membrane and its relation to hemolytic disorders: an optical tweezers study, Biophys. J. 77 (6) (1999) 3085–3095.
[97] M. Dao, C.T. Lim, S. Suresh, Mechanics of the human red blood cell deformed by optical tweezers, J. Mech. Phys. Solids 51 (11–12) (2003) 2259–2280.
[98] S. Suresh, J. Spatz, J. Mills, A. Micoulet, M. Dao, C. Lim, M. Beil, T. Seufferlein, Connections between single-cell biomechanics and human disease states: gastrointestinal cancer and malaria, Acta Biomater. 1 (1) (2005) 15–30.
[99] J. Guck, R. Ananthakrishnan, H. Mahmood, T.J. Moon, C.C. Cunningham, J. Käs, The optical stretcher: a novel laser tool to micromanipulate cells, Biophys. J. 81 (2) (2001) 767–784.
[100] J. Guck, R. Ananthakrishnan, C.C. Cunningham, J. Käs, Stretching biological cells with light, J. Phys. 14 (19) (2002) 4843.
[101] J. Guck, R. Ananthakrishnan, T.J. Moon, C. Cunningham, J. Käs, Optical deformability of soft biological dielectrics, Phys. Rev. Lett. 84 (23) (2000) 5451.
[102] P.B. Bareil, Y. Sheng, A. Chiou, Local stress distribution on the surface of a spherical cell in an optical stretcher, Opt. Express 14 (25) (2006) 12503–12509.
[103] P.B. Bareil, Y. Sheng, Y.-Q. Chen, A. Chiou, Calculation of spherical red blood cell deformation in a dual-beam optical stretcher, Opt. Express 15 (24) (2007) 16029–16034.
[104] A.E. Ekpenyong, C.L. Posey, J.L. Chaput, A.K. Burkart, M.M. Marquardt, T.J. Smith, M.G. Nichols, Determination of cell elasticity through hybrid ray optics and continuum mechanics modeling of cell deformation in the optical stretcher, Appl. Opt. 48 (32) (2009) 6344–6354.
[105] Y.-P. Liu, C. Li, K.-K. Liu, A.C. Lai, The deformation of an erythrocyte under the radiation pressure by optical stretch, J. Biomech. Eng. 128 (6) (2006) 830–836.
[106] F.K. Glenister, R.L. Coppel, A.F. Cowman, N. Mohandas, B.M. Cooke, Contribution of parasite proteins to altered mechanical properties of malaria-infected red

blood cells, Blood 99 (3) (2002) 1060–1063.
[107] S. Suresh, J. Spatz, J. Mills, A. Micoulet, M. Dao, C. Lim, M. Beil, T. Seufferlein, Reprint of: connections between single-cell biomechanics and human disease states: gastrointestinal cancer and malaria, Acta Biomater. 23 (2015) S3–S15.
[108] S.K. Mohanty, A. Uppal, P.K. Gupta, Self-rotation of red blood cells in optical tweezers: prospects for high throughput malaria diagnosis, Biotechnol. Lett. 26 (12) (2004) 971–974.
[109] S.K. Mohanty, K.S. Mohanty, P.K. Gupta, Dynamics of interaction of RBC with optical tweezers, Opt. Express 13 (12) (2005) 4745–4751.
[110] S.K. Mohanty, A. Uppal, P.K. Gupta, Optofluidic stretching of RBCs using single optical tweezers, J. Biophotonics 1 (6) (2008) 522–525.
[111] H. Byun, T.R. Hillman, J.M. Higgins, M. Diez-Silva, Z. Peng, M. Dao, R.R. Dasari, S. Suresh, Y. Park, Optical measurement of biomechanical properties of individual erythrocytes from a sickle cell patient, Acta Biomater. 8 (11) (2012) 4130–4138.
[112] M. Brandao, A. Fontes, M. Barjas-Castro, L. Barbosa, F. Costa, C. Cesar, S. Saad, Optical tweezers for measuring red blood cell elasticity: application to the study of drug response in sickle cell disease, Eur. J. Haematol. 70 (4) (2003) 207–211.
[113] M.M. Brandao, M.d.L.R. Castro, A. Fontes, C.L. Cesar, F.F. Costa, S.T. Saad, Impaired red cell deformability in iron deficient subjects, Clin. Hemorheol. Micro. 43 (3) (2009) 217–221.
[114] K. Fraczkowska, M. Bacia, M. Przybyło, D. Drabik, A. Kaczorowska, J. Rybka, E. Stefanko, S. Drobczynski, J. Masajada, H. Podbielska, et al., Alterations of biomechanics in cancer and normal cells induced by doxorubicin, Biomed. Pharmacother. 97 (2018) 1195–1203.
[115] C.N. Lima, D.S. Moura, Y.S. Silva, T.H. Souza, F.A. Crisafuli, D.C. Silva, J.C. Peres, C.L. Cesar, R.E. de Araujo, A. Fontes, Evaluating viscoelastic properties and membrane electrical charges of red blood cells with optical tweezers and cationic quantum dots–applications to β-thalassemia intermedia hemoglobinopathy, Colloids Surf. B 186 (2020) 110671.
[116] R. Agrawal, T. Smart, J. Nobre-Cardoso, C. Richards, R. Bhatnagar, A. Tufail, D. Shima, P.H. Jones, C. Pavesio, Assessment of red blood cell deformability in type 2 diabetes mellitus and diabetic retinopathy by dual optical tweezers stretching technique, Sci. Rep. 6 (2016) 15873.
[117] A. Pellizzaro, G. Welker, D. Scott, R. Solomon, J. Cooper, A. Farone, M. Farone, R.S. Mushi, M. del Pilar Aguinaga, D. Erenso, Direct laser trapping for measuring the behavior of transfused erythrocytes in a sickle cell anemia patient, Biomed. Opt. Express 3 (9) (2012) 2190–2199.
[118] H.J. Meiselman, Red blood cell aggregation: 45 years being curious, Biorheology 46 (1) (2009) 1–19.
[119] O.K. Baskurt, H.J. Meiselman, Erythrocyte aggregation: basic aspects and clinical importance, Clin. Hemorheol. Micro. 53 (1–2) (2013) 23–37.
[120] D.E. Brooks, Mechanism of red cell aggregation, Blood Cells, Rheology, and Aging, Springer, 1988, pp. 158–162.
[121] S. Asakura, F. Oosawa, On interaction between two bodies immersed in a solution of macromolecules, J. Chem. Phys. 22 (7) (1954) 1255–1256.
[122] P. Bronkhorst, J. Grimbergen, G. Brakenhoff, R. Heethaar, J. Sixma, The mechanism of red cell (dis) aggregation investigated by means of direct cell manipulation using multiple optical trapping, Br. J. Haematol. 96 (2) (1997) 256–258.
[123] M. Khokhlova, E.V. Lyubin, A.G. Zhdanov, A.A. Fedyanin, S.Y. Rykova, I.A. Sokolova, Normal and system lupus erythematosus red blood cell interactions studied by double trap optical tweezers: direct measurements of aggregation forces, J. Biomed. Opt. 17 (2) (2012) 025001.
[124] K. Lee, A. Priezzhev, S. Shin, F. Yaya, I. Meglinski, Characterization of shear stress preventing red blood cells aggregation at the individual cell level: the temperature dependence, Clin. Hemorheol. Micro. 64 (4) (2016) 853–857.
[125] K. Lee, M. Kinnunen, M.D. Khokhlova, E.V. Lyubin, A.V. Priezzhev, I. Meglinski, A.A. Fedyanin, Optical tweezers study of red blood cell aggregation and disaggregation in plasma and protein solutions, J. Biomed. Opt. 21 (3) (2016) 035001.
[126] K. Lee, A.V. Danilina, M. Kinnunen, A.V. Priezzhev, I. Meglinski, Probing the red blood cells aggregating force with optical tweezers, IEEE J. Sel. Top. Quant. 22 (3) (2015) 365–370.
[127] K. Lee, E. Shirshin, N. Rovnyagina, F. Yaya, Z. Boujja, A. Priezzhev, C. Wagner, Dextran adsorption onto red blood cells revisited: single cell quantification by laser tweezers combined with microfluidics, Biomed. Opt. Express 9 (6) (2018) 2755–2764.
[128] T. Avsievich, A. Popov, A. Bykov, I. Meglinski, Mutual interaction of red blood cells assessed by optical tweezers and scanning electron microscopy imaging, Opt. Lett. 43 (16) (2018) 3921–3924.
[129] T. Avsievich, Y. Tarakanchikova, R. Zhu, A. Popov, A. Bykov, I. Skovorodkin, S. Vainio, I. Meglinski, Impact of nanocapsules on red blood cells interplay jointly assessed by optical tweezers and microscopy, Micromachines 11 (1) (2020) 19.
[130] R. Zhu, T. Avsievich, A. Bykov, A. Popov, I. Meglinski, Influence of pulsed He–Ne laser irradiation on the red blood cell interaction studied by optical tweezers, Micromachines) 10 (12) (2019) 853.
[131] T. Avsievich, A. Popov, A. Bykov, I. Meglinski, Mutual interaction of red blood cells influenced by nanoparticles, Sci. Rep. 9 (1) (2019) 5147.
[132] H.P. Fernandes, A. Fontes, A. Thomaz, V. Castro, C.L. Cesar, M.L. Barjas-Castro, Measuring red blood cell aggregation forces using double optical tweezers, Scand. J. Clin. Lab. Inv. 73 (3) (2013) 262–264.
[133] B.-W. Yang, Z. Li, Measuring micro-interactions between coagulating red blood cells using optical tweezers, Biomed. Opt. Express 1 (4) (2010) 1217–1224.
[134] R. Dasgupta, S.K. Mohanty, P.K. Gupta, Controlled rotation of biological microscopic objects using optical line tweezers, Biotechnol. Lett. 25 (19) (2003) 1625–1628.
[135] M.K. Kreysing, T. Kießling, A. Fritsch, C. Dietrich, J.R. Guck, J.A. Käs, The optical cell rotator, Opt. Express 16 (21) (2008) 16984–16992.
[136] M. Kreysing, D. Ott, M.J. Schmidberger, O. Otto, M. Schürmann, E. Martín-Badosa, G. Whyte, J. Guck, Dynamic operation of optical fibres beyond the single-mode regime facilitates the orientation of biological cells, Nat. Commun. 5 (2014) 5481.
[137] R. Dasgupta, S. Ahlawat, R.S. Verma, P.K. Gupta, Optical orientation and rotation of trapped red blood cells with Laguerre-Gaussian mode, Opt. Express 19 (8) (2011) 7680–7688.
[138] X. Liu, J. Huang, Y. Li, Y. Zhang, B. Li, Rotation and deformation of human red blood cells with light from tapered fiber probes, Nanophotonics 6 (1) (2017) 309.
[139] S.J. Parkin, R. Vogel, M. Persson, M. Funk, V.L. Loke, T.A. Nieminen, N.R. Heckenberg, H. Rubinsztein-Dunlop, Highly birefringent vaterite microspheres: production, characterization and applications for optical micromanipulation, Opt. Express 17 (24) (2009) 21944–21955.
[140] Y. Arita, M. Mazilu, K. Dholakia, Laser-induced rotation and cooling of a trapped microgyroscope in vacuum, Nat. Commun. 4 (2013) 2374.
[141] X. Chen, G. Xiao, X. Han, W. Xiong, H. Luo, B. Yao, Observation of spin and orbital rotation of red blood cell in dual-beam fibre-optic trap with transverse offset, J. Opt. (UK) 19 (5) (2017) 055612.
[142] R. Petry, M. Schmitt, J. Popp, Raman spectroscopya prospective tool in the life sciences, Chem. Phys. Chem. 4 (1) (2003) 14–30.
[143] P.J. Lambert, A.G. Whitman, O.F. Dyson, S.M. Akula, Raman spectroscopy: the gateway into tomorrow's virology, Virol. J. 3 (1) (2006) 51.
[144] Harris C.M., This spectroscopic tool is on a new course as scientists find ways of expanding it, Anal. Chem. 74(15) (2002) 433 A438 A.
[145] J. Salter, The effect of radiation trapping of high intensity scattered radiation on multiphonon ionisation rates and resonance fluorescence, J. Phys. B. 12 (24) (1979) L763.
[146] D.V. Petrov, Raman spectroscopy of optically trapped particles, J. Opt. A - Pure Appl. Opt. 9 (8) (2007) S139.
[147] B.R. Wood, P. Caspers, G.J. Puppels, S. Pandiancherri, D. McNaughton, Resonance Raman spectroscopy of red blood cells using near-infrared laser excitation, Anal. Bioanal. Chem. 387 (5) (2007) 1691–1703.
[148] K. Ramser, J. Enger, M. Goksör, D. Hanstorp, K. Logg, M. Käll, A microfluidic system enabling Raman measurements of the oxygenation cycle in single optically trapped red blood cells, Lab Chip 5 (4) (2005) 431–436.
[149] M. Wojdyla, S. Raj, D. Petrov, Absorption spectroscopy of single red blood cells in the presence of mechanical deformations induced by optical traps, J. Biomed. Opt. 17 (9) (2012) 097006.
[150] S. Rao, Š. Bálint, L. del Carmen Frias, D. Petrov, Polarization Raman study of protein ordering by controllable RBC deformation, J. Raman Spectrosc. 40 (9) (2009) 1257–1261.
[151] S. Ahlawat, A. Chowdhury, N. Kumar, A. Uppal, R.S. Verma, P.K. Gupta, Polarized Raman spectroscopic investigations on hemoglobin ordering in red blood cells, J. Biomed. Opt. 19 (8) (2014) 87002.
[152] A.C. De Luca, G. Rusciano, R. Ciancia, V. Martinelli, G. Pesce, B. Rotoli, L. Selvaggi, A. Sasso, Spectroscopical and mechanical characterization of normal and

thalassemic red blood cells by Raman tweezers, Opt. Express 16 (11) (2008) 7943–7957.
[153] M.P. MacDonald, S. Neale, L. Paterson, A. Richies, K. Dholakia, G. Spalding, Cell cytometry with a light touch: sorting microscopic matter with an optical lattice. J. Biol. Reg. Homeos. Ag. 18 (2) (2004) 200–205.
[154] A. Fontes, H. Fernandes, M.L. Barjas-Castro, A. De Thomaz, L.Y. Pozzo, L. Barbosa, C. Cesar, Studying red blood cell agglutination by measuring electrical and mechanical properties with a double optical tweezers, Microsc. Microanal. 12 (S02) (2006) 1758–1759.
[155] M. Brandão, S. Saad, C. Cezar, A. Fontes, F. Costa, M. Barjas-Castro, Elastic properties of stored red blood cells from sickle trait donor units, Vox Sang. 85 (3) (2003) 213–215.
[156] D.C. Silva, C.N. Jovino, C.A. Silva, H.P. Fernandes, M. Milton Filho, S.C. Lucena, A.M.D. Costa, C.L. Cesar, M.L. Barjas-Castro, B.S. Santos, et al., Optical tweezers as a new biomedical tool to measure zeta potential of stored red blood cells, PLoS One 7 (2) (2012) e31778.
[157] M. Barjas-Castro, M. Brandao, A. Fontes, F. Costa, C. Cesar, S. Saad, Elastic properties of irradiated RBCs measured by optical tweezers, Transfusion 42 (9) (2002) 1196–1199.
[158] G.-B. Liao, P.B. Bareil, Y. Sheng, A. Chiou, One-dimensional jumping optical tweezers for optical stretching of bi-concave human red blood cells, Opt. Express 16 (3) (2008) 1996–2004.
[159] J. Lukose, N. Mithun, G. Mohan, S. Shastry, S. Chidangil, Normal saline-induced deoxygenation of red blood cells probed by optical tweezers combined with the micro-Raman technique, RSC Adv. 9 (14) (2019) 7878–7884.
[160] S. Oddos, C. Dunsby, M.A. Purbhoo, A. Chauveau, D.M. Owen, M.A. Neil, D.M. Davis, P.M. French, High-speed high-resolution imaging of intercellular immune synapses using optical tweezers, Biophys. J. 95 (10) (2008) L66–L68.
[161] D.G. Glass, N. McAlinden, O.R. Millington, A.J. Wright, A minimally invasive optical trapping system to understand cellular interactions at onset of an immune response, PLoS One 12 (12) (2017).
[162] X. Wei, B.J. Tromberg, M.D. Cahalan, Mapping the sensitivity of T cells with an optical trap: polarity and minimal number of receptors for Ca2+ signaling, Proc. Natl. Acad. Sci. 96 (15) (1999) 8471–8476.
[163] B. Anvari, J.H. Torres, B.W. McIntyre, Regulation of pseudopodia localization in lymphocytes through application of mechanical forces by optical tweezers, J. Biomed. Opt. 9 (5) (2004) 865–873.
[164] M.D. Mannie, T.J. McConnell, C. Xie, Y.-q. Li, Activation-dependent phases of T cells distinguished by use of optical tweezers and near infrared Raman spectroscopy, J. Immunol. Methods 297 (1–2) (2005) 53–60.
[165] Y. Feng, E.L. Reinherz, M.J. Lang, $\alpha\beta$T cell receptor mechanosensing forces out serial engagement, Trends Immunol. 39 (8) (2018) 596–609.
[166] M. Snijder-Van As, B. Rieger, B. Joosten, V. Subramaniam, C. Figdor, J.S. Kanger, A hybrid total internal reflection fluorescence and optical tweezers microscope to study cell adhesion and membrane protein dynamics of single living cells, J. Microsc. 233 (1) (2009) 84–92.
[167] Å. Holm, T. Sundqvist, Å. Öberg, K.-E. Magnusson, Mechanical manipulation of polymorphonuclear leukocyte plasma membranes with optical tweezers causes influx of extracellular calcium through membrane channels, Med. Biol. Eng. Comput. 37 (3) (1999) 410–412.
[168] M. Yanai, J. Butler, T. Suzuki, H. Sasaki, H. Higuchi, Regional rheological differences in locomoting neutrophils, Am. J. Physiol.-Cell Physiol. 287 (3) (2004) C603–C611.
[169] S.-K. Wang, J.-J. Chiu, M.-R. Lee, S.-C. Chou, L.-J. Chen, N.H. Hwang, Leukocyte–endothelium interaction: measurement by laser tweezers force spectroscopy, Cardiovasc. Eng. 6 (3) (2006) 111–117.
[170] A.E. Ekpenyong, N. Toepfner, C. Fiddler, M. Herbig, W. Li, G. Cojoc, C. Summers, J. Guck, E.R. Chilvers, Mechanical deformation induces depolarization of neutrophils, Sci. Adv. 3 (6) (2017) e1602536.
[171] Y. Liang, G. Liang, Y. Xiang, J. Lamstein, R. Gautam, A. Bezryadina, Z. Chen, Manipulation and assessment of human red blood cells with tunable “tug-of-war” optical tweezers, Phys. Rev. Appl. 12 (6) (2019) 64060.
[172] B.V. Nagesh, R. Pratibha, P. Parthasarathi, S.S. Iyengar, S. Bhattacharya, S. Ananthamurthy, et al., Birefringence of a normal human red blood cell and related optomechanics in an optical trap, J. Biomed. Opt. 19 (11) (2014) 115004.
[173] Y.-T. Wu, A. Chiou, C.-W. Sun, Correlation between tissue oxygenation and erythrocytes elasticity, J. Biophotonics 4 (4) (2011) 224–228.
[174] V. Sheikh-Hasani, M. Babaei, A. Azadbakht, H. Pazoki-Toroudi, A. Mashaghi, A.A. Moosavi-Movahedi, S.N.S. Reihani, Atorvastatin treatment softens human red blood cells: an optical tweezers study, Biomed. Opt. Express 9 (3) (2018) 1256–1261.
[175] F.-l. Mao, Q.-r. Xing, K. Wang, L.-y. Lang, Z. Wang, L. Chai, Q.-y. Wang, Optical trapping of red blood cells and two-photon excitation-based photodynamic study using a femtosecond laser, Opt. Commun. 256 (4–6) (2005) 358–363.
[176] M. Zhou, H. Yang, J. Di, E. Zhao, Manipulation on human red blood cells with femtosecond optical tweezers, Chin. Opt. Lett. 6 (12) (2008) 919–921.
[177] H. Turlier, D.A. Fedosov, B. Audoly, T. Auth, N.S. Gov, C. Sykes, J.-F. Joanny, G. Gompper, T. Betz, Equilibrium physics breakdown reveals the active nature of red blood cell flickering, Nat. Phys. 12 (5) (2016) 513.
[178] I.A. Favre-Bulle, A.B. Stilgoe, E.K. Scott, H. Rubinsztein-Dunlop, Optical trapping in vivo: theory, practice, and applications, Nanophotonics 8 (6) (2019) 1023–1040.
[179] M.-C. Zhong, X.-B. Wei, J.-H. Zhou, Z.-Q. Wang, Y.-M. Li, Trapping red blood cells in living animals using optical tweezers, Nat. Commun. 4 (2013) 1768.
[180] H. Anton, S. Harlepp, C. Ramspacher, D. Wu, F. Monduc, S. Bhat, M. Liebling, C. Paoletti, G. Charvin, J.B. Freund, et al., Pulse propagation by a capacitive mechanism drives embryonic blood flow, Development 140 (21) (2013) 4426–4434.
[181] M. Peralta, E. Steed, S. Harlepp, J.M. González-Rosa, F. Monduc, A. Ariza-Cosano, A. Cortés, T. Rayón, J.-L. Gómez-Skarmeta, A. Zapata, et al., Heartbeat-driven pericardiac fluid forces contribute to epicardium morphogenesis, Curr. Biol. 23 (18) (2013) 1726–1735.
[182] S. Harlepp, F. Thalmann, G. Follain, J.G. Goetz, Hemodynamic forces can be accurately measured in vivo with optical tweezers, Mol. Biol. Cell 28 (23) (2017) 3252–3260.
[183] X. Li, C. Liu, S. Chen, Y. Wang, S.H. Cheng, D. Sun, In vivo manipulation of single biological cells with an optical tweezers-based manipulator and a disturbance compensation controller, IEEE Trans. Robot. 33 (5) (2017) 1200–1212.
[184] H.-C. Liu, Y. Li, R. Chen, H. Jung, K.K. Shung, Single-beam acoustic trapping of red blood cells and polystyrene microspheres in flowing red blood cell saline and plasma suspensions, Ultrasound Med. Biol. 43 (4) (2017) 852–859.
[185] Pappano A., Wier W., Cardiovascular physiology, Mosby Physiology Monograph Series, 2013.
[186] G. Knoener, J.H. Campbell, N.R. Heckenberg, H. Rubinsztein-Dunlop, Formation of an artificial blood vessel: adhesion force measurements with optical tweezers, Optical Trapping and Optical Micromanipulation, 5514 International Society for Optics and Photonics, 2004, pp. 234–245.
[187] P.L. Johansen, F. Fenaroli, L. Evensen, G. Griffiths, G. Koster, Optical micromanipulation of nanoparticles and cells inside living Zebrafish, Nat. Commun. 7 (2016) 10974.
[188] V. Bormuth, A. Jannasch, M. Ander, C.M. van Kats, A. van Blaaderen, J. Howard, E. Schäffer, Optical trapping of coated microspheres, Opt Express 16 (18) (2008) 13831–13844.